In situ synthesis, electrochemical, surface morphological, UV–visible, DFT and Monte Carlo simulations of novel 5-substituted-8-hydroxyquinoline for corrosion protection of carbon steel in a hydrochloric acid solution

M. El Faydy [a], B. Lakhrissi [a], A. Guenbour [b], S. Kaya [c], F. Bentiss [d,e], I. Warad [f], A. Zarrouk [b,*]

[a] Laboratory of Agricultural Resources, Polymer and Process Engineering, Faculty of Sciences, Ibn Tofail University, PO Box 242, 14000 Kenitra, Morocco
[b] Laboratory of Materials, Nanotechnology and Environment, Faculty of Sciences, Mohammed V University, Av. Ibn Battuta, B.P 1014 Rabat, Morocco
[c] Cumhuriyet University, Faculty of Sciences, Department of Chemistry, Sivas, Turkey
[d] Laboratory of Catalysis and Corrosion of Materials, Faculty of Sciences, Chouaib Doukkali University, PO Box 20, M-24000 El Jadida, Morocco
[e] Univ. Lille, CNRS, INRA, ENSCL, UMR 8207, - UMET - Unit of Materials and Transformations, F-59000 Lille, France
[f] Department of Chemistry, AN-Najah National University, P.O. Box 7, Nablus, Palestine

ARTICLE INFO

ABSTRACT

Two new organic compounds based on 8-hydroxyquinoline have been successfully synthesized, and characterized by FT-IR, 1H, ^{13}C NMR and Elemental analysis. The synthesized compounds namely tert-butyl((8-hydroxyquinolin-5-yl)-methyl)-carbamate (BHQC) and Ethyl 3-(((8-hydroxyquinolin-5-yl)-methyl)-amino)-3-oxopropanoate (EHQP) are evaluated as corrosion inhibitors for carbon steel (CS) in 1 M HCl solution using electrochemical techniques, UV — visible and SEM at 298 K. Electrochemical measurements showed that these organic compounds are mixed type inhibitors. The adsorption of both inhibitors on the carbon steel surface followed Langmuir adsorption isotherm. Furthermore, DFT calculations and Monte Carlo simulation were performed to theoretically establish the relationship between molecular structure and inhibition efficiency.

© 2019 Elsevier B.V. All rights reserved.

1. Introduction

In Morocco, the estimation of corrosion costs is approximately 5% of national GNP [1]. Besides corrosion has a negative effect on the environment such as pollution, accidents, dispersion of corrosion products in the environment, in addition to the replacement of corroded installations and equipments, this equates to generate growth cost; these losses could be superior if there was no protection against the corrosion. Carbon steel is one of the main raw materials used in industries and machinery, but unfortunately it corrodes when exposed to different industrial environments. On the other hand, hydrochloric acid is among the most used acids for the removal of undesirable scale and rust in several industrial processes, Because of their aggressiveness, it shows an important corrosive effect on steel [2,3]. Among the preventions used to reduce the corrosion of materials, includes those related to the use of corrosion inhibitors, the choice of appropriate inhibitors depends primarily on the structure [4]. Most of these inhibitors are organic molecules generally include heteroatoms, π-electron and

aromatic rings [5–9]. The protective effect of these organic compounds is related to interactions with metallic surfaces by adsorption [10]. The different types of the attractive forces between the adsorbate and the metal are the physisorption and the chemisorption or a combination of both. The adsorption of inhibitors surface takes place through functional groups and electronic density of donor atoms which tends generally to form a stronger coordination bond and consequently a minimization of corrosion rate [11–15]. 8-hydroxyquinoline derivatives are of immense significance in analytical chemistry, due to their chelating ability toward a great number of metal cations [16,17]. On the other hand, few studies have been carried out in the field of metal protection against corrosion by 8-hydroxyquinoline derivatives. The existing researches obtained by some of 8-hydroxyquinoline derivatives as corrosion inhibitors of carbon steel in acid solutions. Achary et al. [18] have been studied in considerable details that the 3-formyl-8-hydroxyquinoline is an excellent inhibitor of mild steel in hydrochloric acid medium. In another work, Abboud et al. [19] showed that the 5-naphthylazo-8-hydroxyquinoline compound acts as a good inhibitor for the corrosion of mild steel in 1 M HCl solution, reaching about 97.8% at 10^{-3} M. Also, a recent work in our laboratory showed that 8-hydroxyquinoline and its derivatives are excellent inhibitors for carbon

steel in acidic solutions [20–22]. These encouraging results obtained showed that the protection efficiency of all the tested compounds exceeds 90% at 10^{-3} M concentration in 1 M HCl, this leads us to test more compounds of this family. In this contribution, two new compounds based on 8-hydroxyquinoline have been successfully synthesized and characterized using FT-IR, ^{1}H, ^{13}C NMR *spectroscopy* and Elemental analysis. Corrosion inhibition behaviour of carbon steel (CS) in acid media was evaluated by potentiodynamic polarization, electrochemical impedance spectroscopy (EIS), UV–visible spectroscopy and scanning electron microscope (SEM). The temperature effect is also studied. The quantum chemical analysis was carried out using DFT and Monte Carlo simulations and correlated with the inhibiting effect of 5-substituted-8-hydroxyquinolines derivatives.

2. Experimental

2.1. Materials

The chemical composition (wt) of carbon steel used for electrochemical measurements is as follows:

Before each experiment, the surface preparation of the CS specimens was treated with emery paper grade 600 and 1200, in order to obtain a fine surface finishing, cleaned with ethanol and washed with distilled water, and dried in hot air.

The aggressive solution (1 M HCl) is prepared by dilution of analytical grade 37% HCl with distilled water, the concentration range of 5-alkylaminomethyl-8-hydroxyquinoline derivative used was ranged from 10^{-3} to 10^{-6} M; the solution volume is 100 mL.

For the synthesis of *N*-((8-hydroxyquinolin-5-yl)-methyl)-formamide derivatives, All solvents and chemical products of departures used were obtained commercially from Aldrich (France or Spain), NMR spectra were recorded on a model Bruker Avance (300 MHz) for solutions in Me_2SO-d_6, and Chemical shifts are given as δ values with reference to tetramethylsilane (TMS) as internal standard. The progress of the reaction was followed by Thin-Layer Chromatography (TLC) using silica gel 60 F254 (E. Merck) plates with visualization by UV light (254 nm). Silica gel with 0.040–0.063 mm particle size was used as a support in every flash chromatography purification procedure. The infrared spectra were recorded from 400 cm^{-1} to 4000 cm^{-1} on a Bruker IFS 66v Fourier transform spectrometer using KBr pellets. The melting points were determined on an automatic electrothermal IA 9200 digital. Elemental analyses were performed on an Elementar CHN VarioMicro Cube analyzer.

So, the preparation of 5-substituted-8-hydroxyquinoline derivative is outlined in Scheme 1, starting from 5-azidomethyl-8-hydroxyquinoline (**1**) that it was prepared according to the method reported in the literature [23], this latter was reduced into 5-aminomethyl-8-hydroxyquinoline (**2**) by an excess of triphenylphosphine, in the presence of tetrahydrofuran and water.

The condensation of 5-aminomethyl-8-hydroxyquinoline was carried out with diethyl malonate and di-tert-butyl dicarbonate compounds to yield the desired compounds. (See Table 1.)

2.2. Compounds synthesis

2.2.1. Synthesis of 5-aminomethyl-8-hydroxyquinoline (2)

5-Aminomethyl-8-hydroxyquinoline (2) was prepared in our laboratory by the reduction of 5-azidomethyl-8-hydroxyquinoline according to previously described conditions [24].

2.2.2. Synthesis of ethyl-3-(((8-hydroxyquinolin-5-yl)-methyl)-amino)-3-oxopropanoate (3)

To a solution of 5-aminomethyl-8-hydroxyquinoline (0.80 g, 4.7 mmol) in 20 mL of acetonitrile, were added diethyl malonate (0.75 g, 4.7 mmol) and a catalytic amount of triethylamine. The reaction mixture was stirred at 90 °C for 10 h. The excess of acetonitrile was distilled under reduced pressure. The reaction mixture was hydrolyzed with saturated ammonium chloride solution and extracted with CHCl$_3$ (3 × 25 mL). The combined organic layers was dried over anhydrous MgSO$_4$ and filtered. After removal of the solvent, the residue obtained was recrystallized from ethanol to afford ethyl-3-(((8-hydroxyquinolin-5-yl)-methyl)-amino)-3-oxopropanoate (**EHQP**) (**3**) (1.00 g, 74%) as a white solid.

2.2.3. Synthesis of tert-butyl ((8-hydroxyquinolin-5-yl)-methyl)-carbamate (4)

To a suspension of 5-aminomethyl-8-hydroxyquinoline (0.17 g, 1 mmol) in dry Acetonitrile, were added boc-anhydride (0.217 g, 1 mmol) and a catalytic amount of triethylamine. The reaction mixture was heated at 90 °C for 6 h. Reaction completion was monitored by TLC. The excess of acetonitrile was distilled under reduced pressure and the reaction mixture was hydrolyzed with saturated ammonium chloride solution and extracted with CHCl$_3$ (3 × 25 mL). The combined organic phases were washed thrice with 20 mL of saturated aqueous chloride sodium, dried over anhydrous MgSO$_4$, and evaporated under vacuum. The crude product was recrystallized from ethanol to give tert-butyl ((8-hydroxyquinolin-5-yl)-methyl)-carbamate (**BHQC**) (**4**) (0.24 g, 87%) as a white solid. The two synthesized molecules show excellent solubility in polar solvents such as DMSO and ethanol. The toxicity of the two compounds was determined theoretically using appropriate software, we found that the compound BHQC is slightly toxic while the compound EHQP is non-toxic.

The characterization data of the inhibitors are reported in Table 2, the spectra of IR, ^{1}H NMR and ^{13}C NMR are attached to supplementary data.
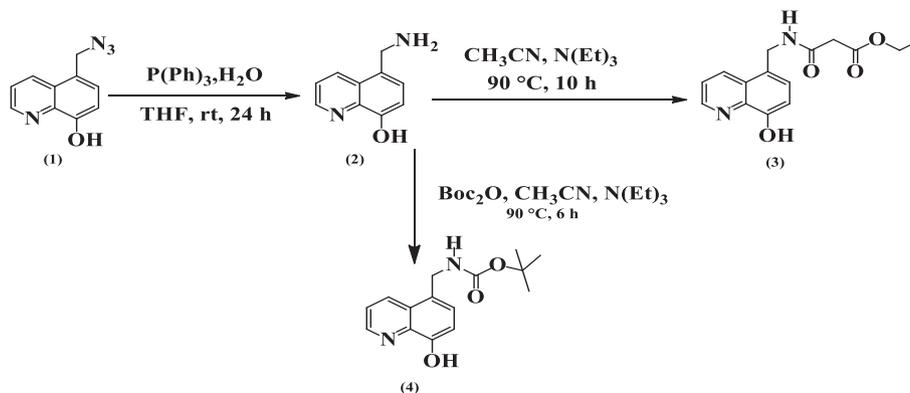
Scheme 1. Synthetic rout for the synthesis of *N*-((8-hydroxyquinolin-5-yl)-methyl)-formamide derivatives (**3**) and (**4**).

Table 1
Chemical composition of carbon steel.

Composition	C	Si	Mn	Al	P	S	Cr	Fe
% wt	0.36	0.10	0.68	0.02	0.01	0.005	0.01	Balance

2.3. Electrochemical methods

Silver chloride (Ag/AgCl) was used as reference electrode with a fine Luggin capillary, which placed close to the working electrode to avoid ohms resistance, and all potentials were reported to silver electrode. The counter electrode was a platinum plate of large surface area. A rectangular working electrode of carbon steel was coated with polyester such that the area exposed to solution was 1 cm^2. All measurements were carried in deaerated solutions under continuously stirred conditions at room temperature (298 ± 2). The measurements were recorded using a Potentiostat/Galvanostat type PGZ 100, at a scan rate of 1 mV/s after its immersion in the test solution for 30 min until reaching steady state.

The corrosion inhibition efficiency is calculated from the corrosion current densities values using the following Eq. (1):

$$\eta_{pp}(\%) = \frac{i_{corr}^0 - i_{corr}}{i_{corr}^0} \times 100 \tag{1}$$

where i_{corr}^0 and i_{corr} are the corrosion current densities values without and with inhibitor, respectively.

The electrochemical impedance spectroscopy measurements (EIS) were obtained out using a transfer function analyzer (VoltaLab PGZ 100); by applying 10 mV amplitude was used to perturb the system in the frequency domain 100 kHz to 10 mHz, the impedance parameters were calculated and fitted by simulation of experimental results to an equivalent circuit using Zview software.

The inhibiting efficiency derived from EIS, η_{EIS} is calculated from the charge transfer resistance values using the following Eq. (2) and is listed in Table 4:

$$\eta_{EIS}(\%) = \frac{R_{ct} - R_{ct}^0}{R_{ct}} \times 100 \tag{2}$$

where R_{ct}^0 and R_{ct} are the charge transfer resistances in the absence and in the presence of inhibitors respectively.

2.4. Scanning electron microscopy (SEM)

The surface of steel before and after immersion in 1 M HCl for 6 h in without and with 10^{-3} M of substituted *N*-((8-hydroxyquinolin-5-yl)-methyl)-formamide was analyzed by Scanning Electron Microscope (SEM) using a JOEL model JSM-5500 microscope. The energy of the acceleration beam employed was 20 kV.

2.5. UV-spectroscopy

UV–visible spectrometry was used in this study on the corrosive solution containing an optimum concentration of all inhibitors before and after 48 h of CS immersion. Jenway UV–visible spectrophotometer (67 series) was used for this analysis.

2.6. Quantum chemical calculations

DFT (Density Functional Theory) is a very important theoretical tools used to give a precise indication on the reactivity and the physicochemical characteristics of a selected chemical species. In recent years, DFT methods have become very indispensable and widespread [25]. In this regard, DFT calculations have been carried out using Gaussian 9.0 Program [26]. The input files of studied compounds were prepared with Gauss View 5.0.8 [27]. A complete optimization was performed up to a higher basis set denoted by 6-31G++ (d,p) since it providing more precise information concerning the determination of electronic properties for a wide range of organic molecules as well, as their geometrical characteristics. Quantum chemical calculations in both gas and aqueous phases were conducted using other levels of theory such as HF and DFT/B3LYP methods with SDD, 6-31++G (d, p) and 6-311++G (d, p) basis sets.

Within the framework the mentioned theory, chemical reactivity descriptors such as chemical hardness, chemical potential, and electronegativity are defined as derivate of electronic energy (E) with respect to number of electron (N) at a constant external potential $\upsilon(r)$. The mathematical equations related to these parameters are mentioned as follows [28,29]:

$$\mu = -\chi = \left(\frac{\partial E}{\partial N}\right)_{\upsilon(r)} \tag{3}$$

$$\eta = \frac{1}{2}\left(\frac{\partial^2 E}{\partial N^2}\right)_{\upsilon(r)} = \frac{1}{2}\left(\frac{\partial \mu}{\partial N}\right)_{\upsilon(r)} \tag{4}$$

Table 2
Characterization data of both synthesized compounds **3** and **4**.

Compounds	Data spectral
Ethyl 3-(((8-hydroxyquinolin-5-yl)-methyl)-amino)-3-oxopropanoate (**EHQP**)	IR (KBr, cm^{-1}): λ = 3468 (quinoline-OH, N—H), 2881-2767 (C—H aromatic), 1632–1876(ketone), 1262 (ester). ^{1}H NMR (300 MHz, Me$_2$SO-d$_6$), δ$_{ppm}$ = 6.998–8.850 (m, 5H, quinoline), 4.721 (s, 2 H, quinoline-CH$_2$-N), 3.655 (s, 2H,-CH$_2$-), 4.182 (m, 2H, O-CH$_2$-), 1.107 (t, 3H, -CH$_3$), 9.796 (s, 1H, N—H). ^{13}C NMR (300 MHz, Me$_2$SO-d$_6$), δ$_{ppm}$ = 15.572 (-CH$_3$), 32.925 (CO-CH$_2$-CO), 45.734 (quinoline-CH$_2$-NH), 65.126 (-CH$_2$-CH$_3$), 110.449, 122.238, 124.919, 133.589, 148.349 (CH-quinoline); 127.845, 128.747, 139.180, 153.757 (C-quinoline), 165.844 (N-C=O), 167.363 (-CH$_2$-C=O). Elemental analysis for C15H16N2O4: Calcd: C, 62.49; H, 5.59; N, 9.72%; Found: C, 62.43; H, 5.58; N, 9.74%. mp 132–134 °C.
Tert-butyl ((8-hydroxyquinolin-5-yl)-methyl)-carbamate (**BHQC**)	IR (KBr, cm^{-1}): λ = 3382 (quinoline-OH, N—H), 2954–2887(CH$_3$), 2380 (C=C aromatic), 1378 (Ter-butyl), 1238 (ester). ^{1}H NMR (300 MHz, Me$_2$SO-d$_6$), δ$_{ppm}$ = 7.013–8.854 (m, 5H, quinoline), 9.843 (s, 1H, -NH), 5.308 (s, 2H, quinoline-CH$_2$-N), 1.286 (s, 9H, C(CH$_3$)$_3$). ^{13}C NMR (300 MHz, Me$_2$SO-d$_6$), δ$_{ppm}$ = 21.785(−(CH$_3$)$_3$), 45.754 (quinoline-CH$_2$-NH$_2$), 72.747 (-C(CH$_3$)$_3$), 110.615, 122.327, 124.362, 127.934, 148.365 (CH-quinoline); 129.470, 133.460, 139.119, 154.022 (C-quinoline); 154.911 (-C=O). Elemental analysis for C15H18N2O3: Calcd: C, 65.68; H, 6.61; N, 10.21%; Found: C, 65.63; H, 6.60; N, 10.23%. mp 118–120 °C

Fig. 1. Potentiodynamic polarization curves for CS in 1 M HCl containing different concentration of **BHQC** and **EHQP** at 298 K.

In order to estimate the chemical reactivity descriptors such as chemical hardness, chemical potential and electronegativity, Pearson and Parr presented the mathematical formulations based on ionization energy and electron affinity values by applying the finite difference approximation [30,31].

$$\eta = \frac{I - A}{2} \tag{5}$$

$$\chi = -\mu = \frac{I + A}{2} \tag{6}$$

where I and A are first vertical ionization energy and electron affinity values of any chemical system, respectively.

Koopman's theorem [32], presents an alternative molecular orbital theory method for estimating the ionization energies and electron affinities of organic molecules. This theorem based on the fact that, the negative of the highest occupied molecular orbital energy and the negative of the lowest unoccupied molecular orbital energy correspond to ionization energy and electron affinity, respectively ($-E_{HOMO} = I$ and $-E_{LUMO} = A$). As consequence of this theorem, chemical hardness and chemical potential can be defined as:

$$\chi = -\mu = \left(\frac{-E_{HOMO} - E_{LUMO}}{2} \right) \tag{7}$$

$$\eta = \left(\frac{E_{HOMO} - E_{LUMO}}{2} \right) \tag{8}$$

Subsequently, another parameter to estimate that is the inverse of the global hardness under the name of global softness and expressed

via following Eq. (9) [33]:

$$\sigma = \frac{1}{\eta} \tag{9}$$

The global electrophilicity index (ω) invented by Parr et al. [34] is a descriptor of reactivity linked to electronegativity and chemical hardness, in addition, electrophilicity index used to determine several parameters like toxicity and corrosion inhibition performance of molecules. On the other hand, nucleophilicity (ε) is defined as the inverse of the electrophilicity. The mathematical expression of this index is given by:

$$\omega = \frac{\mu^2}{2\eta} = \frac{\chi^2}{2\eta} \tag{10}$$

$$\varepsilon = \frac{1}{\omega} \tag{11}$$

8-Hydroxyquinoline and its derivatives are organic bases (presence of an imine and amine ($=N$, NH) group in the studied molecules). This means that the addition of an acid to the aqueous solution of any of these organic molecules will transform the neutral molecule into a cation. In 1 M HCl, this is the supporting electrolyte used in this study and has a pH value of close at zero, the molecules of 8-hydroxyquinoline and its derivatives protonate. Hence it is important to investigate the chemical properties of the protonated species of studied compounds. In this context, proton affinities of organic molecules can be readily determined. As is known, proton affinity of chemical species provides remarkable clues about their basicity. The proton affinities (PA) of inhibitors can be calculated via the following equation:

$$PA = E_{(pro)} - \left(E_{(non-pro)} + E_{H^+} \right) \tag{12}$$

Table 3
Polarization parameters for CS in 1 M HCl in the absence and presence of different concentration of BHQC and EHQP.

Medium	Conc. [M]	$-E_{corr}$ vs. Ag/AgCl (mV)	i_{corr} ($\mu A/cm^2$)	$-\beta_c$ (mV/dec)	β_a (mV/dec)	η_{pp} (%)
Blank	00	454	551.40	98	85.6	–
EHQP	10^{-3}	457	78.52	97	87.2	85.8
	10^{-4}	456	123.48	123	98.9	77.6
	10^{-5}	462	195.00	120	102.0	64.6
	10^{-6}	455	285.10	124	87.1	48.3
BHQC	10^{-3}	460	26.49	100	98.1	95.2
	10^{-4}	459	46.90	90	87.4	91.5
	10^{-5}	467	54.46	97	94.0	90.1
	10^{-6}	467	68.92	98	92.4	87.5
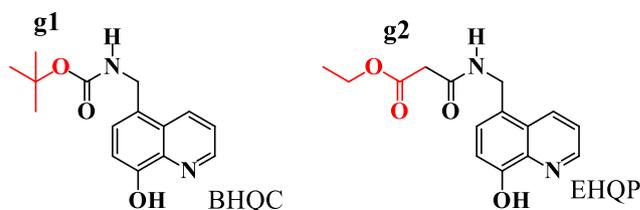
Fig. 2. The difference in structure between BHQC and EHQP (**g1** and **g2**).
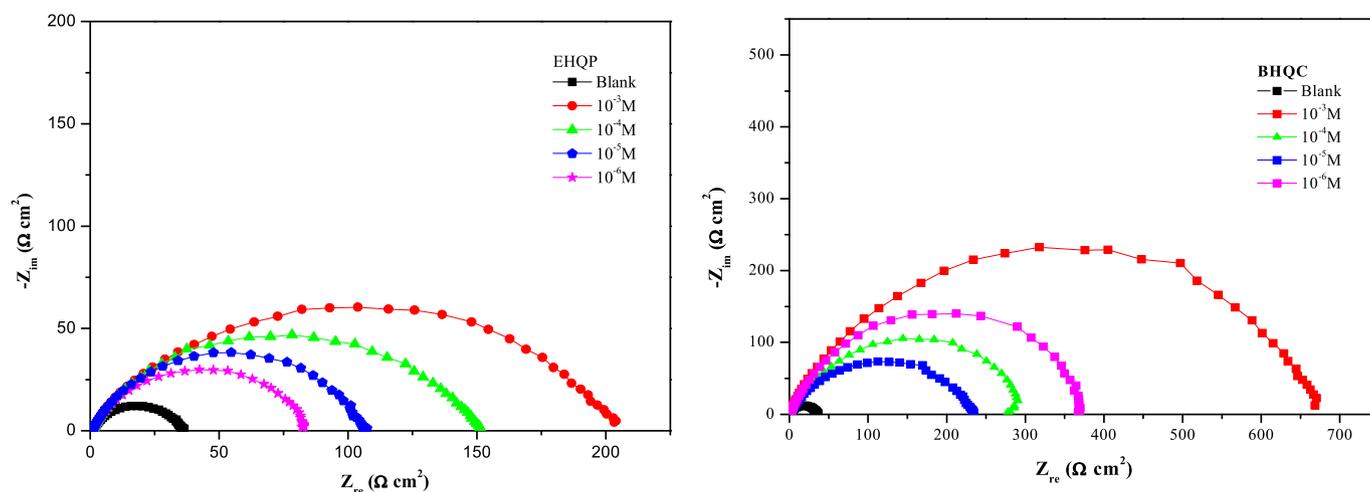
Fig. 3. Nyquist plots for CS in 1 M HCl solution containing different concentrations of BHQC and EHQP at 298 K.

where, $E_{(pro)}$ and $E_{(non-pro)}$ are the energies of the protonated and non-protonated inhibitors, respectively. E_{H^+} is the energy of H^+ which was estimated as:

$$E_{H^+} = E_{(H_3O^+)} - E_{(H_2O)} \tag{13}$$

where, $E_{(H_2O)}$ is the total energy of a water molecule and $E_{(H_3O^+)}$ is the total energy of the hydronium ion.

2.7. Monte Carlo simulations

The adsorption progress of 5-substituted-8-hydroxyquinoline derivatives on clean iron surface is carried by performing Monte Carlo simulations using adsorption locator module (Accelrys, San Diego, CA, USA), using state of the art software, known as Material Studio 7.0. The Fe (110) crystal surface was chosen for this simulation and according to the literature [35], it is the most stable surface. Firstly, the iron surface was then optimized to the energy minimum. Then, the Fe (110) surface was simulated with a six-layer slab model. In this model, there were 100 iron atoms in each layer representing a (10 × 10) unit cell, and a 40 Å vacuum region between two adjacent layers to ensure the repeated slabs decoupled. A cutoff distance of 1.85 nm with a spline switching function was applied for the non bond interactions (i.e., electrostatic interactions and van der Waals). A low-energy adsorption site is identified by performing out a Monte Carlo search of the configuration space of the additives on the iron surface system as the temperature is slowly decreased (simulated annealing). This approach was repeated to identify further local energy minima. During the simulation, adsorbate molecules are randomly rotated and translated around the iron surface. The configuration that results from one of these steps can be accepted or rejected according to the selection rules of the Metropolis Monte Carlo method. For all simulations, the COMPASS (condensed phase optimized molecular potentials for atomistic simulation studies) force field were used to optimize the structures of all components of the system of interest [36].
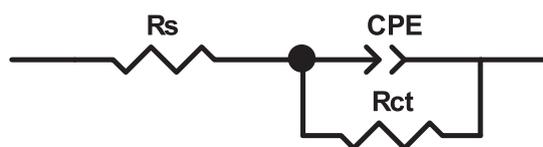
Fig. 4. Equivalent circuit applied for impedance analysis.

3. Results and discussion

3.1. Polarization measurements

Both anodic and cathodic polarization curves obtained in the absence and presence of various concentrations of BHQC and EHQP are presented in Fig. 1. Preliminary results indicate that the examined compounds decrease in both cathodic and anodic current densities, this effect is more pronounced with increasing concentration, and their presence does not cause any significance shift in the E_{corr} value, Moreover, the parallel cathodic Tafel curves suggested that the hydrogen evolution is activation controlled and the reduction mechanism is not affected by the presence of BHQC and EHQP. In the anodic part, it is clear that the anodic reaction is also inhibited, but the organic compounds did not show a corrosion inhibition effect at CS for the potential values higher than (−250 mV/Ag/AgCl), indicating the desorption of the adsorbed molecules from the CS surface, this potential can be defined as the desorption potential.

The extrapolation of the linear segments of cathodic and anodic curves permitted to determine the electrochemical parameters as corrosion potential (E_{corr}), corrosion current density (i_{corr}) and Tafel slopes (β_c and β_a), these Tafel data along with calculated inhibition efficiency (η_{pp} %) are given in Table 3.

The analysis of Table 3 shows that the value of η_{pp} (%) increased with BHQC and EHQP concentrations reaching a maximum (85%) for the high concentration of BHQC and (95%) for the high concentration of EHQP. The higher inhibition efficiency of BHQC can be attributed to the ability of this inhibitor to chemisorb on the metal surface more than the inhibitor EHQP. In addition, a comparison of the values of the Tafel slopes (β_c), showed that, with respect to the blank, a change irregularly with the addition of organic compounds, indicating the effects of the 5-aminomethyl-8-hydroxyquinoline derivatives on the kinetics of hydrogen evolution. This can be explained by the diffusion or the barrier effect [37]. However, the values of the slopes of the anodic Tafel lines (β_a) are changed with the presence of both inhibitors, which reflects the influence of the 5-aminomethyl-8-hydroxyquinoline derivatives on the kinetics of the anodic mechanism [38]. These results confirm that BHQC and EHQP exhibited both cathodic and anodic inhibition effects. Consequently BHQC and EHQP can be classified as mixed-type inhibitors in 1 M HCl.

The inhibition efficiency differences would probably originate in the substituents bound to 5-aminomethyl-8-hydroxyquinoline while the 5-aminomethyl-8-hydroxyquinoline moiety remains constant (Fig. 2). This can be explained on the basis of +I and —I effect of the substituents. The tert-butoxy group (**g1**) in BHQC acts as an electron donating group conjugated to nitrogen and oxygen heteroatoms, and therefore
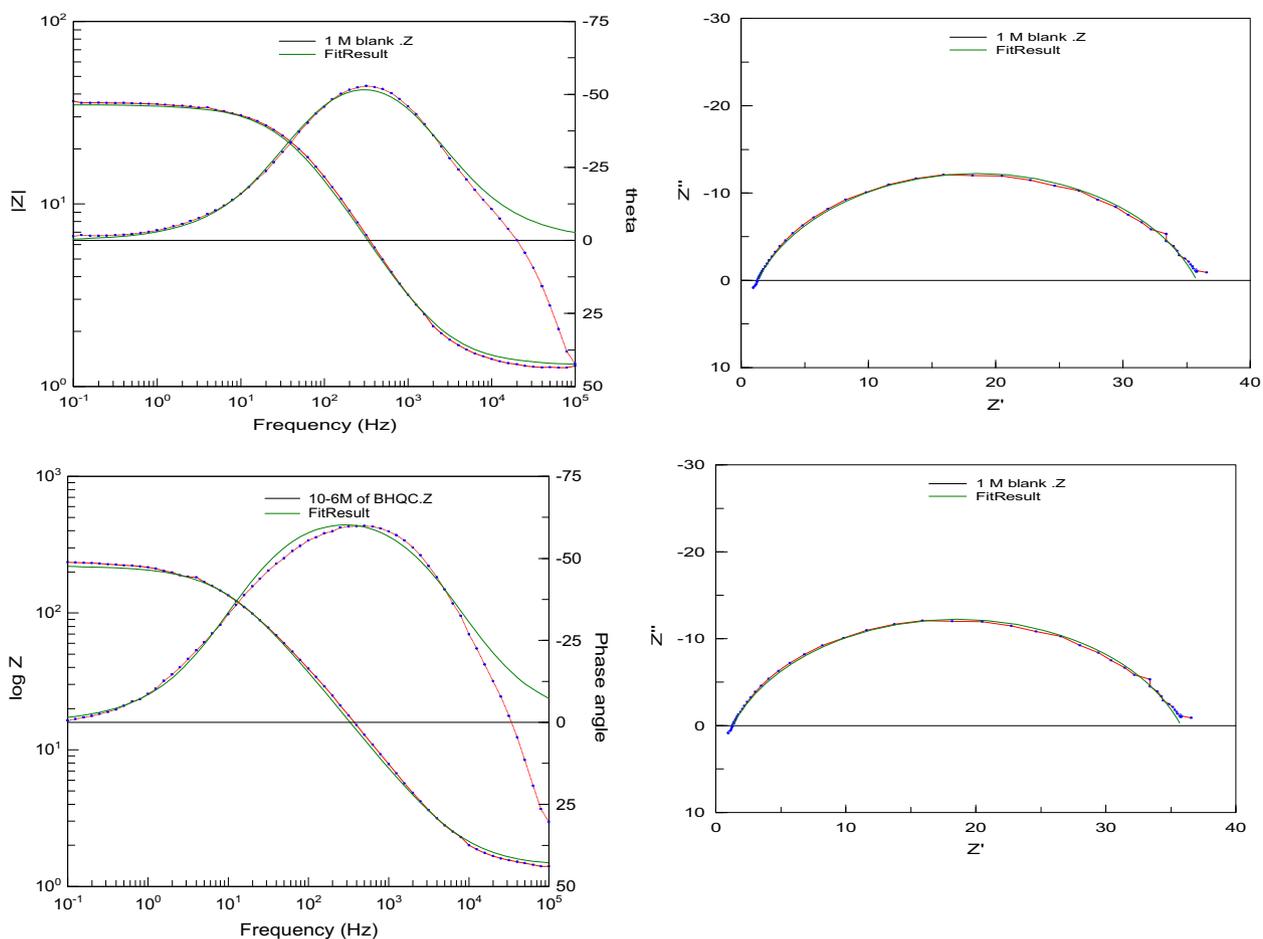
Fig. 5. Representative example of EIS Nyquist and Bode diagrams simulated in 1 M HCl with 10^{-4} M of BHQC at 298 K.

the electron density of the delocalized π electron on the quinoline ring increases, and consequently stronger adsorption on the metal surface.

The carboethoxy group (**g2**) in EHQP represents an electron-withdrawing group which reducingthe electron density on the quinoline ring, which results low adsorption on the metal surface.

3.2. Electrochemical impedance spectroscopy (EIS)

In order to confirm the results obtained by the potentiodynamic polarization curves and to study the adsorption and inhibition mechanism in detail of BHQC and EHQP, electrochemical impedance spectroscopy

measurements were used, the corresponding Nyquist plots for CS in the absence and presence of various concentrations of BHQC and EHQP at 298 K are shown in Fig. 3. It is evident from these plots that the impedance response of CS has gradually increased after the addition of BHQC and EHQP to the corrosive solution and therefore the protection efficiency increases. All Nyquist plots exhibit a single capacitive loop at high frequency (HF), this is in conforming with the observation of Bode plots representation, the HF capacitive loop is generally attributable to charge transfer of the corrosion process. It is notable that the Nyquist plots are not perfect semicircles which ascribed to the frequency dispersion of interfacial impedance [39], this phenomenon is a
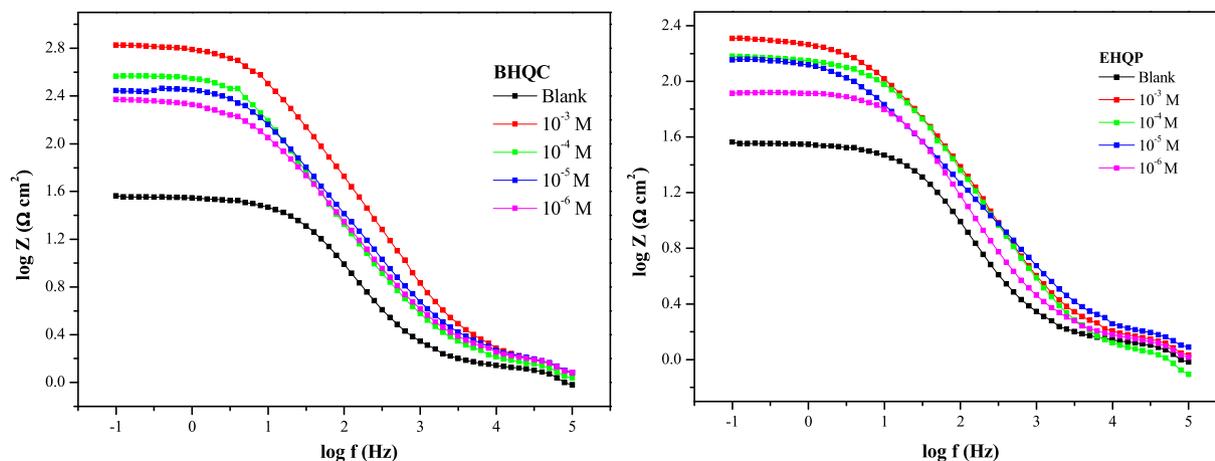
Fig. 6. The Bode plots for CS in 1 M HCl solutions containing different concentrations of BHQC and EHQP at 298 K.
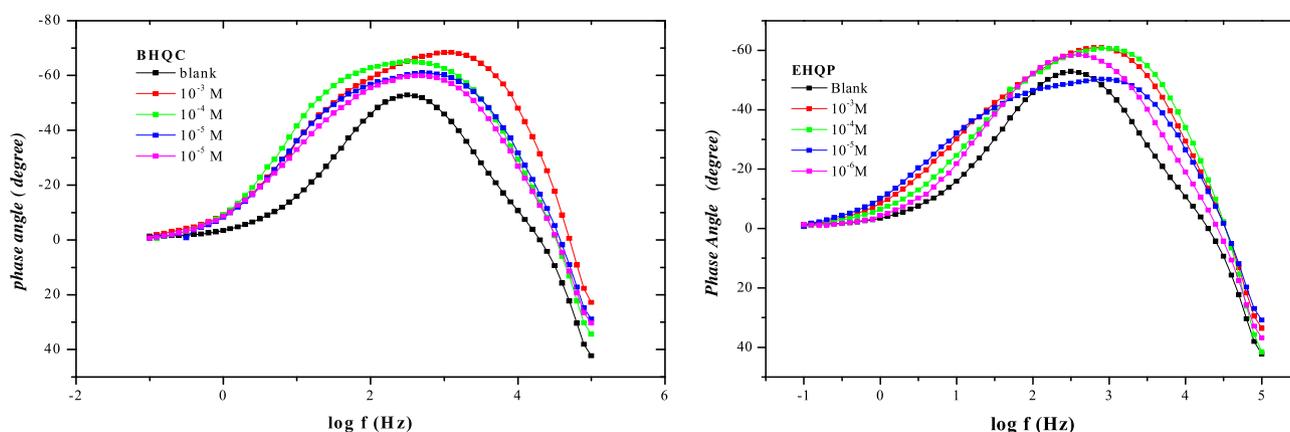
Fig. 7. The phase angle plots for CS in 1 M HCl solution containing different concentrations of BHQC and EHQP at 298 K.

related to the roughness of the electrode surface, the chemical heterogeneity of surface and mass transport process. Also the similar shape of impedance spectra for uninhibited and inhibited solutions suggesting that there is no change in the corrosion mechanism. All impedance data are simulated (representative example Fig. 5) using the equivalent circuit presented in Fig. 4, which contains of R_s reflects the solution resistance, R_{ct} is the charge transfer resistance, and CPE is the constant phase elements for the double layer. As it was demonstrated before [40], the best fit of the impedance plots was obtained by constant phase elements rather than an ideal capacitor C_{dl}, this replacement was intended to modeling the frequency dispersion behavior. The impedance of the CPE is defined by [41]:

$$Z_{CPE} = A^{-1}(i\omega)^{-n} \tag{14}$$

Where A is the CPE constant in $(\Omega^{-1}s^n cm^{-2})$, $\boldsymbol{n}$ is the CPE exponent determining the phase shift (ranges from 0 to 1), $\boldsymbol{i}^2 = -1$ is an imaginary number and $\boldsymbol{\omega}$ is the angular frequency in (rad s^{-1}) ($\omega = 2\pi f$, where f is the frequency) and subsequently the values of double layer capacitance are determined by the following mathematical formula [42]:

$$C_{dl} = \left(A_d R_{ct}^{1-n} \right)^{1/n} \tag{15}$$

With regard to the relaxation time (τ), which indicates the time required for returning of the charge distribution to equilibrium after an
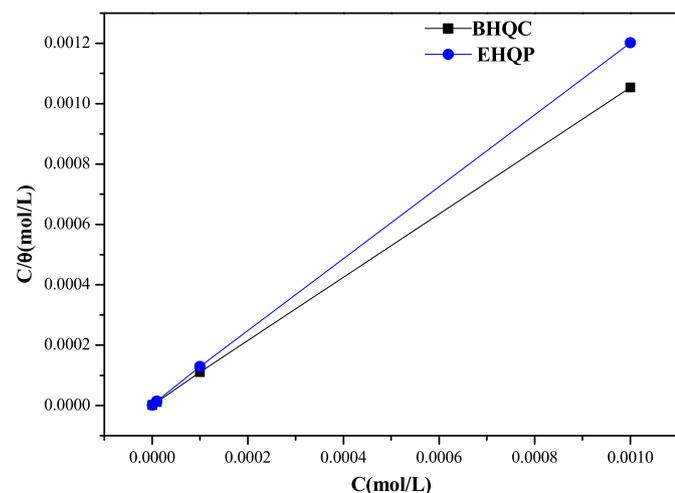
electric perturbation and determined by the following equation [43]:

$$\tau = C_{dl}R_{ct} \tag{16}$$

The fitted parameters for both uninhibited solutions and in 1 M HCl solution containing BHQC and EHQP are summarized in Table 4. Including also, the margins of error for all parameters already set forth, they are average approximately 10^{-2} which indicates that the fitted data have good agreement with the experimental data.

Addition of increasing concentrations of BHQC and EHQP increases R_{ct}, and consequently enhances η_{EIS} till reaching their maximum values at optimum concentration 10^{-3} M ($R_{ct} = 202$ (Ω cm^2), $\eta_{EIS} = 83\%$ for EHQP and $R_{ct} = 669$ (Ω cm^2), $\eta_{EIS} = 94\%$ for BHQC, The increase in R_{ct} values in presence of 5-aminomethyl-8-hydroxyquinoline derivatives are related to the adsorption of BHQC and EHQP on the metal surface leading to the formation of protective film at the metal/solution interface. Meanwhile, remarkable decreases in the values of the C_{dl} with the increasing of concentration of BHQC and EHQP, which indicate decrease in local dielectric constant and/or an increase in the thickness of the electrical double layer. However, the values of $\boldsymbol{n}$ are situated between 0.7 and 0.8, which suggests a reduction of a surface inhomogeneity as a result of the 5-aminomethyl-8-hydroxyquinoline molecules adsorption on CS surface [44]. Moreover, the addition of inhibitors provides higher $\boldsymbol{\tau}$ values, this increase can be explained by the rate of adsorption process is approximately slow [45].

The Bode plots (log (Z) vs.log (f)) and angle plots (phase angle (α) vs.log (f)) for CS in 1 M HCl solution without and with different concentrations of 5-aminomethyl-8-hydroxyquinoline derivatives are given in Figs. 6 and 7, three distinct segments can be observed, at very high frequencies, log(Z) values tend to approach zero and the phase angle falls above zero 0°, These are the responses to resistive behavior and related to the electrolyte resistance. For an intermediate frequency range, the slopes of Bode impedance magnitude plots at this region, S, and the maximum phase angles, α_{max} are given in Table 5. log [Z] vs. log with slope values (from -0.640 to -0.788) and the phase angle values (from $-50.24°$ to $-68.41°$). Based on the existing literature, a pure capacitor's characteristic would result in a slope of -1 and a phase angle of $-\pi/2$ [46]. However the deviations obtained account for the deviation from an ideal capacitive response, the small differences that exist between S and α_{max} to the ideal capacitive values could be related to the slowing down of the rate of dissolution with time. Finally, at the low frequency region, the resistive behavior of the electrode increases, and log (Z) becomes independent of frequency [47].

3.3. Adsorption isotherm

Frequently, the first reaction of inhibitors in acid solution that happens is to adsorb on the metal surface, this action depends upon the

Fig. 8. Langmuir adsorption plot for BHQC and EHQP on CS in 1 M HCl solution.
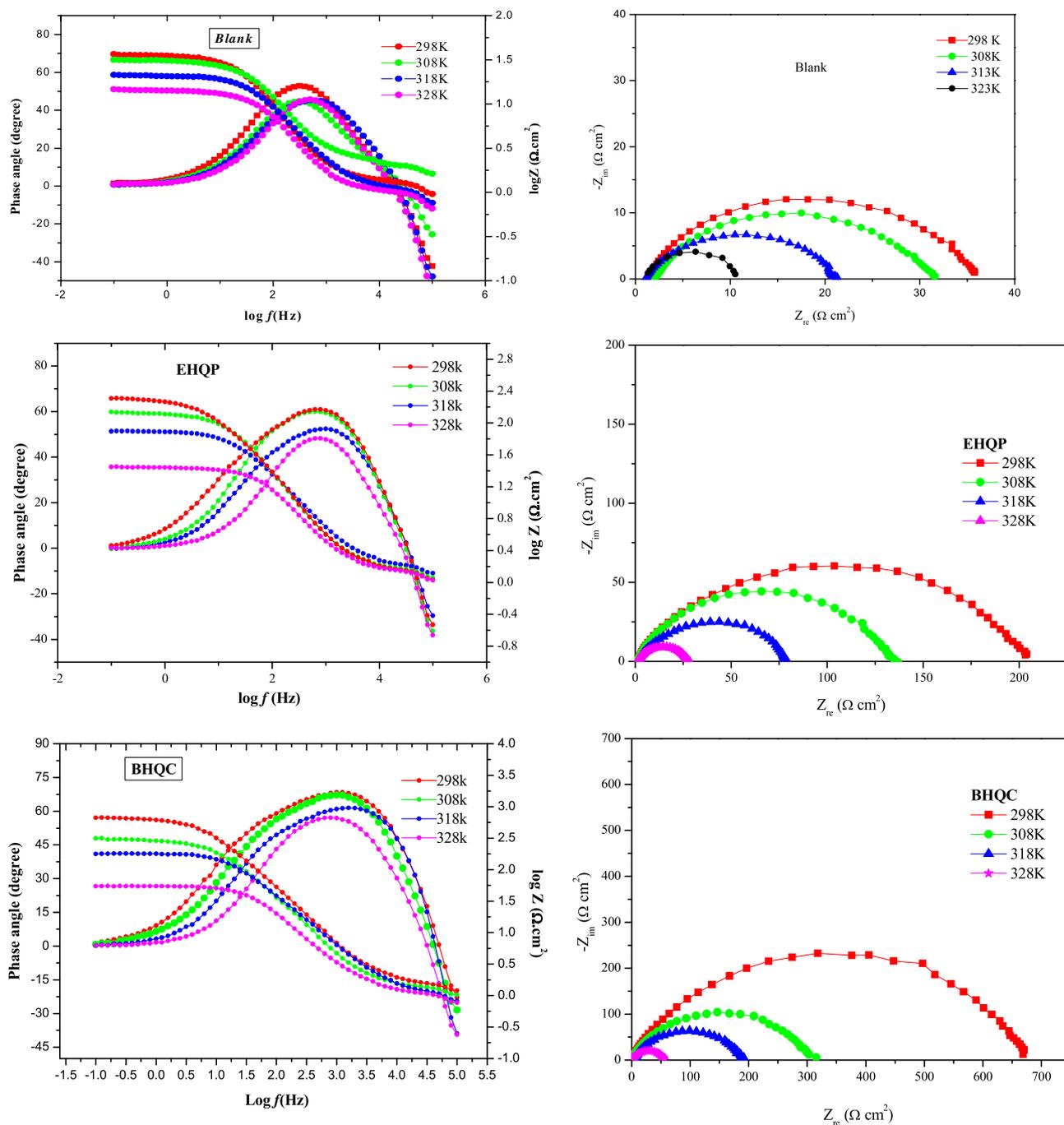
Fig. 9. The phase angle, Bode and Nyquist plots for *CS* in *1 M* HCl + 10^{-3} M of the synthesized inhibitors at different temperatures.

electronic properties of metal and the species involved. The adsorption isotherm allows gaining a better understanding of inhibitor mechanism between the tested compounds and metal surface. For this, the coverage surface (θ) can be determined from the impedance measurements by the following expression θ = η_{EIS}/100. The high accordance between the experimental results and isotherm models was obtained using Langmuir adsorption isotherm. Based on this isotherm θ is related to concentration inhibitor C_{inh} by the following Eq. (17) [48].

$$\frac{C_{inh}}{\theta} = \frac{1}{K_{ads}} + C_{inh} \qquad (17)$$

where K_{ads} is the equilibrium constant of the adsorption process, their values were calculated from the intercept of the Langmuir isotherm

plot. This constant is permitted to determine the standard Gibbs energy of adsorption, ΔG_{ads}°, by the following Eq. (18) [49,50],

$$K_{ads} = \frac{1}{55.5} \exp\left(\frac{-\Delta G_{ads}^{\circ}}{RT}\right) \qquad (18)$$

where 55.5 value correspond to the water concentration in solution by mol/L, R is the universal gas constant (8.3143 J K^{-1} mol^{-1}), and T is the absolute temperature (298 K).

For BHQC and EHQP, the plots for C_{inh}/θ versus C give a straight line with all the correlation coefficients (R^2) are equal to 0.999 meaning that the adsorption of BHQC and EHQP on steel surface obeys Langmuir adsorption isotherm. But, a slight increase in the slope from unity for
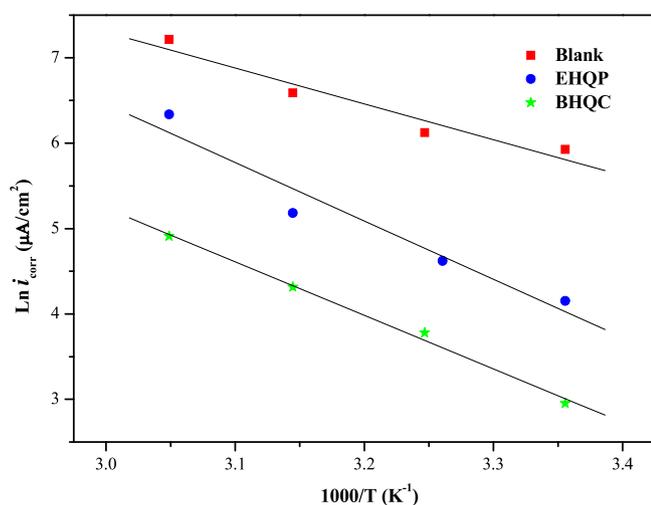
Fig. 10. Variation of Ln (i_{corr}) as a function versus ($10^3/T$) on CS in 1 M HCl to calculate the activation energy of corrosion process in the absence and presence of inhibitors BHQC and EHQP.

BHQC and EHQP may be due to the interactions between organic molecules and iron atoms as represented in Fig. 8.

The calculated values of K_{ads} and ΔG_{ads}° at each organic compound are given in Table 6. It is found that all the values of the standard free energy of adsorption ΔG_{ads}° are negative. However, the literature review reveals that the values of ΔG_{ads}° approximate to −20 (kJ mol^{-1}) or less negative are coherent with physisorption, while those around −40 kJ mol^{-1} or more negative are corresponded with chemisorptions [51], in our case, ΔG_{ads}° values for EHQP and BHQC are −40.655 and −42.727 kJ mol^{-1}, respectively. The obtained values are of slightly more negative than −40 kJ mol^{-1} signifies that the adsorption mechanism of the inhibitor molecules on CS in 1 M HCl solution is typical of chemisorption, indicating that the chemical interactions predominate for the adsorption of BHQC and EHQP molecules on the steel surface. These chemical interactions of BHQC and EHQP molecules in 1 M HCl medium are attributable primarily to free electrons on the nitrogen and oxygen atoms as well π-electrons of the quinoline rings with the vacant 3d orbitals of the iron atom. The relative absorbability of BHQC molecules is greater than that of EHQP; this is in accordance with the results obtained from electrochemical techniques.
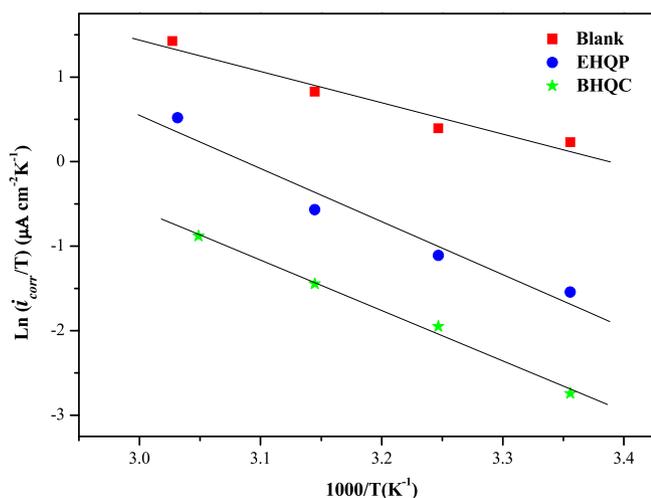
Fig. 11. Transition-state plots for CS in 1 M HCl in absence and presence of 10^{-3} M of inhibitors BHQC and EHQP.

3.4. Effect of temperature

In order to study the effect of temperature on the corrosion inhibition with and without the synthesized compounds, the electrochemical impedance spectroscopy measurements are used with the range of temperature 303, 313, 323 and 333 K in the absence and presence of 10^{-3} M for BHQC and EHQP (Fig. 9). All the recorded impedance spectra of CS immersed in 1 M HCl with and without the compounds studied exhibits only one capacitive loop with one capacitive time constant in the Bode-phase plot, and the diameters of the semicircle decreases with increasing the temperature. The corresponding fitted parameters are calculated using Zview software at various temperatures on the basis of the equivalent circuit offered previously, and presented in Table 7. The temperature rise results in decrease of R_{ct} values. This is linked to the increase of the rate of metal dissolution, or else to desorption of the EHQP and BHQC molecules at metal/electrolyte interfaces and therefore to the decrease of surface coverage degree, However, the values of R_{ct} in the presence of BHQC compound at high temperatures are greater when compared to the EHQP compound, whose molecules are also similar and differ only by the g_1 and g_2 group, This could mean that the g_1 increases the delocalization of electron density in the compound, which makes the molecule more stable and therefore a higher protective effect.

Furthermore, the *n* value remains relatively constant after 308 K and its increase in the absence of the inhibitor molecule is very little compared to it in the presence of the inhibitor molecule. Its increase with the presence of the inhibitor molecule may be connected, from an energetic point of view, with the inhibitor's adsorption at the most active sites on the metal surface and their isolation so that the surface as a whole behaves as one of lower heterogeneity and could have been connected with steric hindrance and different orientation of the molecules [52]. The double layer capacitance C_{dl} values increased with temperature increase, generally, this can be related with the thickness of the layer of adsorbed inhibitor molecules on the electrode surface [53]. Moreover, similar tendency was found for *A* values for all temperatures studied both in uninhibited and inhibited solutions, they are lower than those in the uninhibited acid. It is concluded that the BHQC and EHQP inhibitors acts as temperature-dependent inhibitors.

The temperature investigations are necessary, but they do not give all the information required for the adsorption character elucidation. In this case, the corrosion current density in the absence and presence of synthesized compounds at various temperatures are calculated from the polarization resistance (R_{ct}) using the following Eq. (19) [54,55] and values obtained are given in Table 7.

$$i_{corr} = RT(zFR_{ct})^{-1} \tag{19}$$

where z is the valence of iron (z = 2), F is the Faraday constant (F = 96,485 coulomb).

In the case, the activation thermodynamic parameters have been used to understand the inhibition mechanism; they are estimated from Arrhenius equation and transition state Eqs. (20) and (21) [56].

$$i_{corr} = A \exp\left(\frac{-E_a}{RT}\right) \tag{20}$$

$$i_{corr} = \frac{RT}{Nh} \exp\left(\frac{\Delta S_a}{R}\right) \exp\left(\frac{-\Delta H_a}{RT}\right) \tag{21}$$

where *A* is the Arrhenius pre-exponential factor, E_a is the apparent activation corrosion energy, R is the universal gas constant, *T* is the absolute temperature, *h* is Plank's constant, *N* is Avogadro's number, ΔS_a is the entropy of activation and ΔH_a is the enthalpy of activation.

As shown in the Fig. 10 the relation between the logarithm of the corrosion current and 1000/T in medium 1 M HCl without and with the addition of synthesized compounds at 10^{-3} M gives straight lines with slopes of $\Delta E_a/R$, the estimated values of the apparent activation
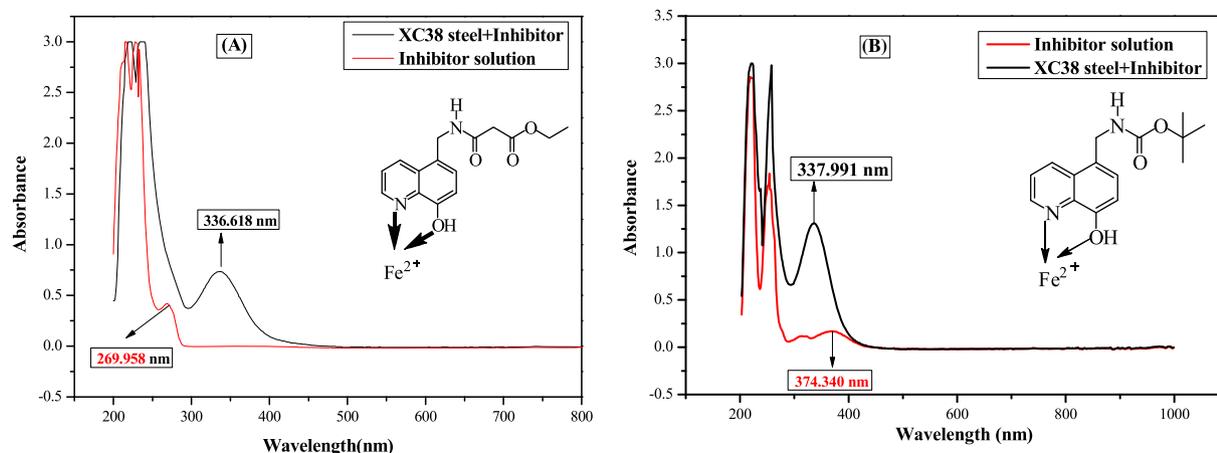
Fig. 12. UV–visible spectra of 1 M HCl solution containing 10^{-3} M of inhibitors before (red) and after (red) 48 h of CS immersion, (A) EHQP and (B) BHQC. (For interpretation of the references to colour in this figure legend, the reader is referred to the web version of this article.)

energy using Eq. (20), are given in Table 8. The comparison among them show that the value of the activation energy for blank solution is lower (34.89 kJ mol^{-1}) than inhibited solution (52.13 or 56.79 kJ mol^{-1}), the results show that addition of BHQC and EHQP in 1 M HCl decreases the dissolution of CS and this hindrance to dissolution is attributable strong electrostatic effects between BHQC and EHQP molecules and the metal surface. But, Fan Zhang explained that the increase in activation energy cannot consider as decisive because of competitive adsorption with water whose removal from the surface requires also some activation energy [57].

It can be estimated the values of standard entropy and enthalpy for CS corrosion in 1 M HCl in absence and with both synthesized compounds using the above formula 21. Fig. 11 shows the plot of Ln (i_{corr}/T) against 1000/T, three straight lines are obtained with the slope of (-ΔH_a/R) and intercept (Ln(R/Nh) + ΔS_a/R), concerning the results shown in Table 8. The values obtained of ΔH_a are higher in the presence of BHQC and EHQP than that in blank solution. Generally, the positive sign of ΔH_a attributed to the endothermic nature of the corrosion

process. The examination of the literature show that the enthalpy of a physisorption process is lower than 40 kJ mol^{-1} while the enthalpy of a chemisorption process gets close to 100 kJ mol^{-1} [58].

In this case, the absolute values of enthalpy superior to 40 but <100 kJ mol^{-1} suggests that the mode of adsorption of BHQC and EHQP on the metal surface is combination of physisorption and chemisorption. As regards the entropy, it is used to describe the phenomenon of ordering and disordering of system, the value of ΔS_a in the absence of inhibitor is negative and tends to increase in presence of BHQC and EHQP (Table 8). This reveals that an increase in disorder at the time when the reactants are transformed to activated complexes. Also, this may be connected to the adsorption of organic molecules was accompanied by desorption of water molecules from the metal surface [59].

3.5. UV–visible spectroscopy

With the aim of developing and confirming the possibility of the formation of *N*-((8-hydroxyquinolin-5-yl)-methyl)-formamide-Fe
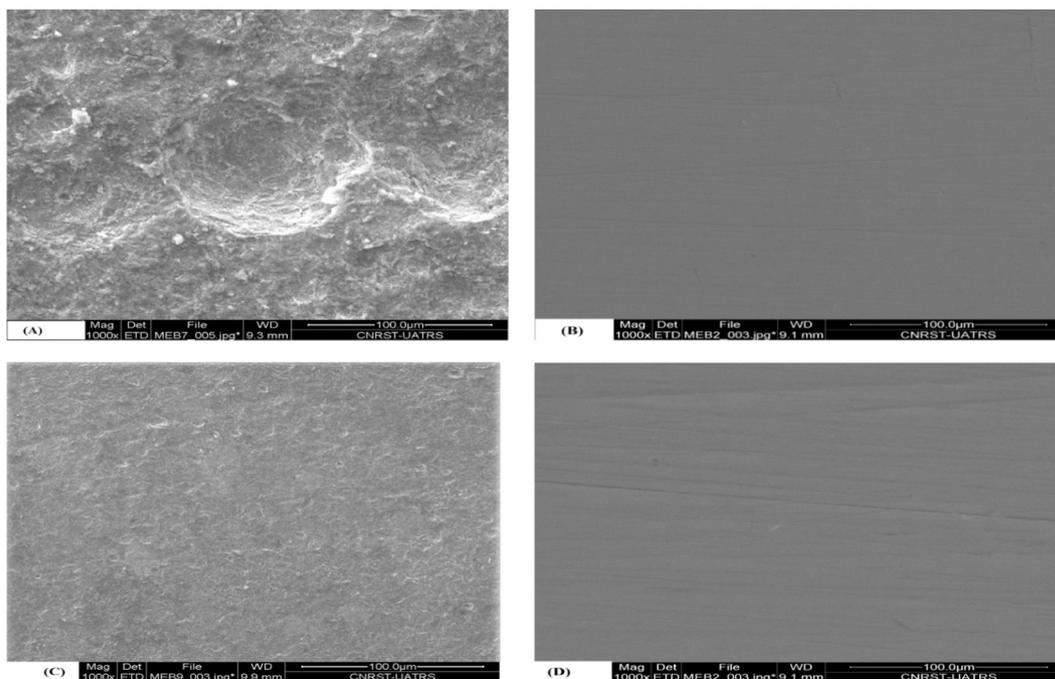
Fig. 13. SEM images of CS: (A) after immersion for 6 h in 1 M HCl, (B) before immersion, (C) after immersion in 1 M HCl solution in presence of 10^{-3} M of EHQC, (D) after immersion in 1 M HCl solution in presence of 10^{-3} M of BHQC.

Inhibitors	Optimized Structure	HOMO	LUMO	ESP
EHQP				
BHQC				
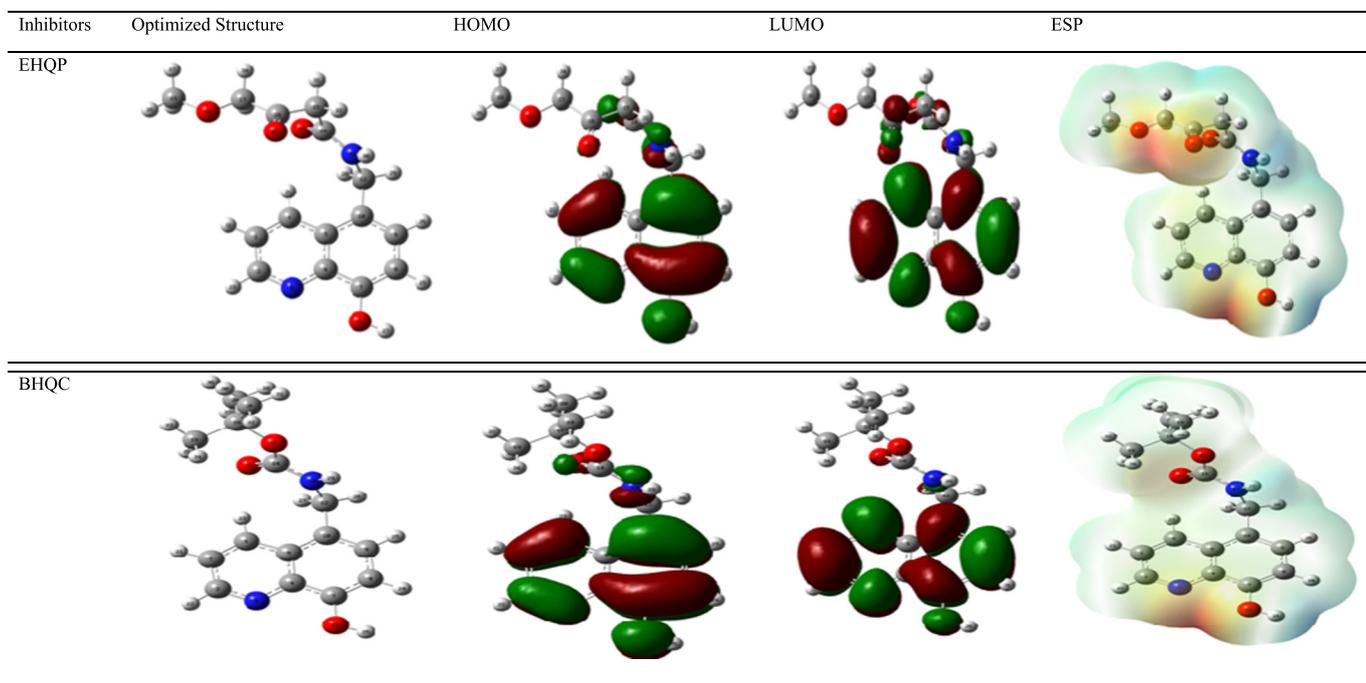
Fig. 14. The optimized structures, HOMOs, LUMOs and electrostatic potential structures of non protonated inhibitor molecules using DFT/6-311++G** calculation level.

complex, UV–Visible absorption spectra obtained from 1 M HCl solution containing 10^{-3} M of BHQC and EHQP before and after 48 h of carbon steel immersion are shown in Fig. 12 for (A) EHQP and (B) BHQC. All curves show that the intensity of the absorbance peak was increased in the presence of organic compounds.

The electronic absorption spectra of EHQP before the steel immersion (A, red curve) exhibit absorption peaks in the range 200–250 nm, corresponding to the π–π* transitions in the quinoline ring, also another

band at around 270 nm is shifted to a higher value (336.618 nm) in case of CS + EHQP inhibitor, indicating that the interaction between EHQP and Fe^{2+} ions in the solution and their intensity greater than that obtained for EHQP only. These results show the formation of a complex between the Fe^{2+} ions and EHQP molecules in hydrochloric acid solution.

The comparison between UV–visible absorption spectra for BHQC before and after of CS immersion (Fig. 12B), demonstrates that there was no significant difference in the overall shape of the spectra in the
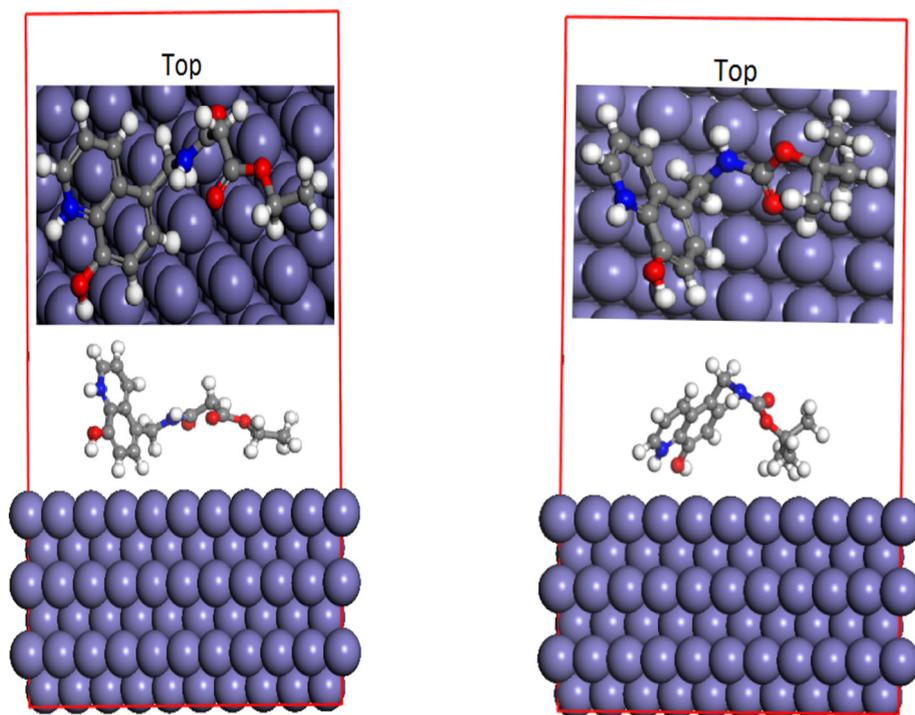
Fig. 15. Top and Side views of the most stable low energy configurations for the adsorption of BHQC (right) and EHQP (left) molecules on Fe (110) interface obtained using Monte Carlo simulations.

Table 4
Calculated EIS parameters from equivalent circuit for CS in 1 M HCl for various concentrations of BHQC and EHQP.

Medium	Conc (M)	R_s (Ω cm^2)	R_{ct} (Ω cm^2)	CPE		C_{dl} (μF cm^{-2})	τ (ms)	η_{EIS} (%)	θ
				10^4 A (Ω^{-1} S^{n}cm^2)	n				
Blank	00	1.303 ± 0.045	34 ± 0.092	4.33 ± 0.015	0.785 ± 0.004	136.86	0.0047	–	–
EHQP	10^{-3}	1.225 ± 0.071	202 ± 0.049	2.82 ± 0.080	0.706 ± 0.004	85.51	0.0173	83.2	0.832
	10^{-4}	1.040 ± 0.069	150 ± 0.053	2.94 ± 0.090	0.725 ± 0.004	89.98	0.0135	77.3	0.773
	10^{-5}	1.169 ± 0.055	104 ± 0.062	3.0 ± 0.0849	0.776 ± 0.003	110.27	0.0115	67.1	0.671
	10^{-6}	1.412 ± 0.086	83 ± 0.0550	3.30 ± 0.059	0.800 ± 0.003	135.00	0.0112	59.0	0.590
BHQC	10^{-3}	1.328 ± 0.076	669 ± 0.026	0.69 ± 0.015	0.779 ± 0.002	28.78	0.0192	94.9	0.949
	10^{-4}	1.393 ± 0.056	374 ± 0.052	1.29 ± 0.002	0.776 ± 0.003	53.98	0.0202	90.9	0.909
	10^{-5}	1.493 ± 0.059	300 ± 0.039	1.44 ± 0.093	0.799 ± 0.003	65.32	0.0196	88.7	0.887
	10^{-6}	1.401 ± 0.061	231 ± 0.098	2.52 ± 0.006	0.725 ± 0.003	85.37	0.0197	85.0	0.850

range 200–250 nm. Furthermore, the last band at 374 nm, which corresponds to n-π* of the lone pair of electrons on the quinoline nitrogen, oxygen atoms and/or carbonyl group, this band is shifted to a lower value at 337.991 in case of carbon steel + BHQC inhibitor, with an increase in absorbance from 0.164 to 1.292. According to Abboud et al. [60], a displacement in of the absorption maximum (λ_{max}) and/or a change in the value of absorbance demonstrate the formation of a complex between the two species in solution; these data provide strong evidence for the possibility of the complex formation between Fe^{2+} and BHQC in 1 M HCl.

3.6. Scanning electron microscopy investigation

The surface morphology of working electrode after immersion in 1 M HCl for 6 h in without and with 10^{-3} M of synthesized compounds were examined using SEM and shown in Fig. 13(A–D). The specimen surface in 1 M HCl solution Fig. 13A was strongly damaged as compared to that before the immersion (Fig. 13B) due to attack of acid. But this damage of the surface is considerably reduced and become smoother and with less pitting in the presence of compounds EHQP and BHQC (Fig. 13C–D). As a result of the formation protective layer at metal electrolyte interfaces, indicating that the inhibitor molecules can be adsorbed on the metal surface and protects it.

3.7. Mechanism of inhibition

In acid media, the synthesized compounds may be protonated to provide cationic species, predominantly attacking the nitrogen atoms. On the other hand, the existing chloride ions in the solution are more readily adsorbed on iron surface which brings about a negative charge favoring the adsorption of BHQC and EHQP cationic forms (BHQCH$^+$ and EHQPH$^+$) through electrostatic interactions (physical adsorption). In addition, the neutral form molecules of BHQC and EHQP may be absorbed through the sharing of electrons between nitrogen and oxygen atoms and π- electron interactions between the quinoline ring of the molecules such as to form a bond with the vacant 3d orbitals of

Table 5
The slopes of the Bode impedance magnitude plots at intermediate frequencies (S) and the maximum phase angles α_{max} in 1 M HCl in the absence and presence of different concentrations of BHQC and EHQP.

Medium	Conc (M)	-α_{max} (deg)	-S
Blank	00	52.89	0.640
BHQC	10^{-3}	68.41	0.788
	10^{-4}	65.41	0.676
	10^{-5}	60.93	0.681
	10^{-6}	59.82	0.732
EHQP	10^{-3}	60.94	0.680
	10^{-4}	60.67	0.697
	10^{-5}	58.57	0.660
	10^{-6}	50.24	0.682

the iron [61]. The substituent tert-butoxy (g_1) is a strong electron donor group which participates in electrons delocalization, leading to mesomeric forms, this accounts stabilization of the BHQC molecules, as depicted in the following Scheme 2. While this effect is not observed on EHQP molecules, signifying that BHQC molecules are better inhibitors than EHQP molecules, which is in fact experimentally verified.

3.8. Quantum chemical calculations

The protective effects of two 8-hydoxyquinolin-5-substituted on the corrosion of CS were investigated by quantum chemical and Monte Carlo simulations approach. The calculated quantum chemical parameters such as dipole moment, electronegativity (χ), chemical potential (μ), hardness (η), nucleophilicity (ϵ), softness (σ), global electrophilicity (ω), highest occupied molecular orbital energy (E_{HOMO}), lowest unoccupied molecular orbital energy (E_{LUMO}) and the energy gap between E_{HOMO} and E_{LUMO} (ΔE) are important tools and very used to correlate between the molecular structure and the corrosion protection [62,63]. All calculated parameters in case non-protonated and protonated of 8-hydroxyquinoline-5-substituted in gas phase and aqueous solution are presented in Tables 9–12. It is has reported that the reactivity of a molecule mainly depends on molecular orbital distribution, the energy of HOMO is connected with the electron donating ability of a molecule, the higher the level of HOMO energy the more the molecule is likely to give electrons to appropriate acceptor molecules with low energy and empty molecular orbital. Also, the molecules with high E_{HOMO} values are considered a good corrosion inhibitor. On the contrary, the energy of LUMO indicates the ability of the molecule to accept electrons, the lower the value of E_{LUMO}, the more probable it is that the molecule accepts electrons. On the other hand, it was shown that the organic molecules give not only electrons to the unoccupied d orbital of the metal surface, but can also accept electron from the d orbital of the metal leading to the formation of a feedback bond. The existing data show that the trend of the E_{HOMO} is BHQC > EHQP, while BHQC < EHQP for E_{LUMO}, except of protonated EHQP and BHQC species in the gas phase at all Basis Set. According to the literature [64], it has been reported that the inhibition efficiency increases with the increasing E_{HOMO} values. In the light of this information, considering E_{HOMO} values given in Tables 9–12, the inhibition efficiency ranking for synthesized inhibitors can be given as: BHQC > EHQP in good agreement with the experimental data most especially in aqueous solution, except of E_{HOMO} values for protonated EHQP and BHQC species in the gas phase at all Basis.

Fig. 14 shows the results of the optimized structures, molecular electrostatic potentials (ESP), HOMO and LUMO orbital distributions for

Table 6
Free energy for the adsorption of different inhibitors in 1 M HCl.

Inhibitor	K_{ads}	R^2	Slopes	ΔG_{ads}° (KJ/Mol)
BHQC	556,247.77	0.999	1.05	−42.727
EHQP	243,273.48	0.999	1.19	−40.655

Table 7
Electrochemical impedance spectroscopy results for CS in 1 M HCl without and with 10^{-3} M of the synthesized compounds at different temperatures.

Medium	Temp (K)	R_s (Ω cm^2)	R_{ct} (Ω cm^2)	CPE 10^4 A (Ω^{-1} S^{n}cm^2)	n	C_{dl} (μF cm^{-2})	τ (ms)	i_{corr} (μA/cm^2)	E (%)
Blank	298	1.303 ± 0.045	34.200 ± 0.920	4.330 ± 0.152	0.785 ± 0.004	136.86	0.0047	375.4	–
	308	1.331 ± 0.057	29.020 ± 0.745	5.000 ± 0.121	0.792 ± 0.003	175.83	0.0051	457.3	–
	318	1.202 ± 0.045	18.820 ± 0.821	6.710 ± 0.019	0.793 ± 0.005	214.34	0.0040	727.9	–
	328	1.415 ± 0.046	10.400 ± 0.185	8.451 ± 0.080	0.795 ± 0.008	249.31	0.0025	1358.8	–
EHQP	298	1.225 ± 0.070	202.00 ± 0.493	2.820 ± 0.080	0.706 ± 0.004	85.510	0.0173	63.6	83.1
	308	1.395 ± 0.095	131.00 ± 0.076	3.052 ± 0.005	0.761 ± 0.004	115.21	0.0151	101.3	77.8
	318	1.887 ± 0.970	77.010 ± 0.025	3.501 ± 0.005	0.768 ± 0.003	117.59	0.0090	177.9	75.6
	328	1.639 ± 0.050	25.040 ± 0.081	3.800 ± 0.008	0.810 ± 0.004	127.52	0.0031	564.4	58.5
BHQC	298	1.328 ± 0.076	669.00 ± 0.262	0.689 ± 0.015	0.779 ± 0.002	28.78	0.0192	19.2	94.9
	308	1.302 ± 0.065	303.00 ± 0.076	1.032 ± 0.026	0.775 ± 0.076	37.78	0.0114	43.8	90.2
	318	1.453 ± 0.050	183.10 ± 0.084	1.393 ± 0.052	0.783 ± 0.005	50.25	0.0092	74.8	89.7
	328	1.308 ± 0.040	54.080 ± 0.020	1.420 ± 0.003	0.836 ± 0.001	54.63	0.0029	135.8	80.8

BHQC and EHQP. As can be seen in Fig. 14, the HOMO densities for the two molecules are located on the 8-hydroxyquinoline moiety also in on N-C=O group attached to the ring. The HOMO orbitals of the both molecules are located mainly on the 8-hydroxyquinoline ring.

The energy gap ($\Delta E = E_{\text{HOMO}} - E_{\text{LUMO}}$) between E_{LUMO} and E_{HOMO} energies is another fundamental parameter which indicates the reactivity tendency of a molecule toward the metal surface and this quantity allows to measure of the stability of the formed complex on the iron surface. The fact that ΔE decreases the reactivity of inhibitor molecules increases consequently an increase in the inhibition efficiency [65]. As can be seen from Tables 9–12, ΔE value of inhibitors follows the order BHQC > EHQP, which suggest that EHQP has the lowest reactivity compared with BHQC, which is agreement with results obtained in experimental part, except those of protonated EHQP and BHQC species in the gas phase and at the HF/SDD, DFT/6-31++G (d,p) and DFT/6-311++G (d,p) levels of basis, who showed the opposite. In such complex corrosion system, quantum chemical parameters calculated from theoretical simulations some time not be compatible with experimental observations. As we found above, all calculated parameters by theoretical models in case of protonated molecules in the gas phase are not compatible with the experimental data.

The global electronegativity (χ) is one of the most important boundary parameters which gives information on the about the prediction and comparison of corrosion inhibition efficiencies of molecules. This quantity for any molecules presents its electron pulling power and the molecules with high electronegativity values do not easily release electrons, which imply that molecules with the least value of electronegativity are expected to be good corrosion inhibitors. In the light of to the calculated electronegativity values using various calculation levels and mentioned in the Tables 9–12, it can be said that the inhibition efficiency of BHQC is higher than that EHQP in all cases with the exception of protonated molecules in gas phase, this is similar to the observations mentioned above.

Hardness and softness are chemical concepts closely linked with HOMO –LUMO energy gap, According to Maximum Hardness Principle [66], chemical hardness can be measured the stability of chemical molecules also, hard molecules which have high HOMO –LUMO energy gap cannot act as good corrosion inhibitor. Softness is assigned to measure of polarizabilities of molecules and it should be noted that soft molecules which have low HOMO – LUMO energy gap act good corrosion inhibitors because they can easily give electrons to metals. In Tables 9–12, the hardness and softness values of both inhibitors are reported. Considering the results given in mentioned tables, one can noted the corrosion inhibition ranking of both inhibitors based on their hardness and softness values follow the order: BHQC > EHQP.

Electrophilicity and nucleophilicity are important parameters that indicate the electronic properties of the studied molecules and used to evaluate the efficiencies of the inhibitor molecules. The electrophilicity parameter represents the electron-accepting capability of a molecule. Whereas, nucleophilicity denotes the tendency to donate electrons with a molecule, it should be noted that a molecule that has great electrophilicity value is powerless in terms of the protection against corrosion, while a molecule that has large nucleophilicity value is considered as a good corrosion inhibitor. Although a few inconsistent exist in the ranking of nucleophilicity and electrophilicity values with experimental results, especially for protonated molecules in the gas phase. Considering to the results given in Tables 9–12, it can be said that the agreement has been obtained with laboratory findings.

Thereafter, the values obtained from the electronegativity and Chemical hardness are exploited to determine another parameter named the number of electrons transferred; this later was estimated according to Sanderson's electronegativity equalization principle. Thus, the value of electron transferred from corrosion inhibitor to iron atom can be expressed via following Eq. (22):

$$\Delta N_{\max} = \frac{\chi_{Fe} - \chi_{inh}}{2\left(\eta_{Fe} + \eta_{inh}\right)} \tag{22}$$

where $\Delta N_{\max}$ is the fraction of electron transferred between iron atom and inhibitor molecule. χ_{Fe} and χ_{inh} are electronegativity of iron and electronegativity of inhibitor, respectively. η_{Fe} and η_{inh} represent the chemical hardness value of iron and chemical hardness value of inhibitor, respectively. According to Hard Soft Acid Base (HSAB) [67] theory, iron is considered as is considered a Lewis acid. Pearson reported that the difference in electronegativity drives the electron transfer and the sum of the hardness parameters acts as a resistance. The corresponding theoretical values for the electronegativity and chemical hardness of bulk iron are of the order $\chi_{Fe} = 7$ eV and $\eta_{Fe} = 0$, respectively, by

Table 8
Kinetic parameters of activation for the adsorption of BHQC and EHQP in 1 M HCl on the CS.

Medium	R^2	E_a (kJ mol^{-1})	ΔH_a (kJ mol^{-1})	ΔS_a (J mol^{-1} K^{-1})
Blank	0.97	34.89	30.79	−93.23
EHQP	0.97	56.79	52.22	−36.34
BHQC	0.99	52.13	49.53	−53.67
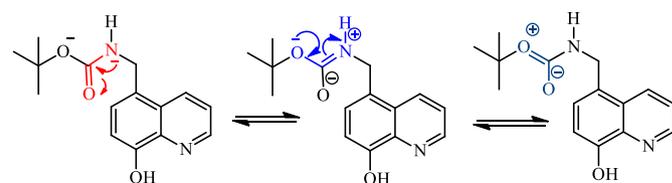
Scheme 2. The mesomeric effect in BHQC molecule.

Table 9

Calculated quantum chemical parameters for non-protonated 5-substituted-8-hydroxyquinline molecules in gas phase (eV).

	E_{HOMO}	E_{LUMO}	I	A	ΔE	χ	μ	η	σ	ω	ε
HF/SDD											
EHQP	−8.41410	1.89801	8.41409	−1.89801	10.31211	3.25804	−3.25804	5.15605	0.19394	1.02935	0.97147
BHQC	−8.27260	2.02590	8.27259	−2.02590	10.29850	3.12334	−3.12334	5.14925	0.19420	0.94725	1.05568
HF/6-31++G**											
EHQP	−8.29165	0.90234	8.29165	−0.90234	9.19398	3.69465	−3.69465	4.59699	0.21753	1.48472	0.67353
BHQC	−8.13600	0.96819	8.13600	−0.96819	9.10419	3.58390	−3.58390	4.55209	0.21968	1.41082	0.70881
HF/6-311++G**											
EHQP	−8.32022	0.87077	8.32022	−0.87077	9.19099	3.72472	−3.72472	4.59550	0.21760	1.50947	0.66248
BHQC	−8.17273	0.92302	8.17273	−0.92302	9.09575	3.62486	−3.62486	4.54787	0.21988	1.44459	0.69224
DFT/SDD											
EHQP	−6.11989	−1.67240	6.11989	1.67242	4.44746	3.89616	−3.89616	2.22373	0.44969	3.41319	0.29298
BHQC	−6.02410	−1.57070	6.02410	1.57065	4.45345	3.79738	−3.79738	2.22673	0.44909	3.23796	0.30884
DFT/6-31++G**											
EHQP	−6.13159	−172,030	6.13159	1.72031	4.41127	3.92595	−3.92595	2.20564	0.45338	3.49403	0.28620
BHQC	−6.04778	−163,680	6.04778	1.63677	4.4110	3.84228	−3.84228	2.20550	0.45341	3.34688	0.29879
DFT/6-311++G**											
EHQP	−6.10111	−168,820	6.10111	1.68820	4.41291	3.89466	−3.89466	2.20645	0.45322	3.43728	0.29093
BHQC	−6.05540	−166,970	6.05540	1.66970	4.38569	3.86255	−3.86255	2.19285	0.45603	3.40181	0.29396

supposing that for a metallic bulk I = A because they are softer than the neutral metallic atoms. The fraction of electron transferred (ΔN_{max}) for both inhibitors was calculated and listed in Tables 13 and 14. The donor or acceptor molecules can be distinguished by considering the value of ΔN, for the molecule acceptor, this fraction of electrons transferred is usually positive number while that for electron donors is attributed to a negative number. In addition, the protection efficiency increases with increasing electron donating ability of these molecules to the metal surface. In the same direction, it has been reported by others that if the value of $\Delta N < 3.6$ eV, the inhibition efficiency increased with increasing electron donating ability at the metal/solution interface [68]. In our case, these obtained values of ΔN_{max} reported in Tables 13 and 14 are all smaller than 3.6 eV indicating that the 5-substutued-8-hydroxyquinoline derivatives are electrons donors with varying degrees, and the mild steel surface is the acceptor which promotes interactions between them facilitating the formation of an adsorption layer that prevent the corrosion process.

Starting from the charge transfer model for donation and back-donation of charges, Gomez and al. [69] suggested that an electronic back-donation process may also determine the interaction between the inhibitor molecule and the metal surface. In this context, if both the electron transfer to the molecule and back-donation from the molecule occurs simultaneously, the energy change is directly proportional to the hardness of the molecule as mentioned in the following Eq. (23):

$$\Delta E_{b-d} = -\frac{\eta}{4} \tag{23}$$

The equation below involves that when $\eta > 0$ or $\Delta E_{b-d} < 0$, back-donation from the molecule to metal is energetically favoured. However, the obtained results in Tables 13 and 14 shows that $\Delta E_{b-d} < 0$, this means that the charge transfer to a molecule followed by back-donation from the molecule is energetically favorable. Assuming that the protection efficiency should increase when there's more adsorption of the molecule on the metal surface. Therefore the protection efficiency should increase when the stabilization energy that results from the interaction between the metal surface and inhibitor increases. On inspection of Tables 13 and 14 it is observed that the trend of the ΔE_{b-d} is in accordance with the inhibition efficiency order obtained from experimental data for both inhibitors, this is not same trend for protonated

Table 10

Calculated quantum chemical parameters for non-protonated 5-substituted-8-hydroxyquinline molecules in aqueous solution (eV).

	E_{HOMO}	E_{LUMO}	I	A	ΔE	χ	μ	η	σ	ω	ε
HF/SDD											
EHQP	−8.51206	1.73338	8.51206	−1.73338	10.24540	3.38934	−3.38934	5.12272	0.19521	1.12124	0.89187
BHQC	−8.46907	1.76195	8.46907	−1.76195	10.23100	3.35356	−3.35356	5.11551	0.19548	1.09924	0.90972
HF/6-31++G**											
EHQP	−8.34689	1.12738	8.34689	−1.12738	9.47426	3.60975	−3.60975	4.73713	0.21110	1.37534	0.72709
BHQC	−8.32267	1.09418	8.32267	−1.09418	9.41685	3.61424	−3.61424	4.70842	0.21239	1.38717	0.72089
HF/6-311++G**											
EHQP	−8.38444	1.07976	8.38444	−1.07976	9.46419	3.65234	−3.65234	4.73210	0.21132	1.40948	0.70948
BHQC	−8.36131	1.04683	8.36131	−1.04683	9.40814	3.65724	−3.65724	4.70407	0.21258	1.42168	0.70339
DFT/SDD											
EHQP	−6.20506	−1.82670	6.20506	1.82671	4.37835	4.01589	−4.01589	2.18917	0.45679	3.68344	0.27149
BHQC	−6.19935	−1.82240	6.19935	1.82236	4.37699	4.01085	−4.01085	2.18849	0.45694	3.67535	0.27208
DFT/6-31++G**											
EHQP	−6.18220	−1.83350	6.18220	1.83351	4.34869	4.00786	−4.00786	2.17434	0.45991	3.69375	0.27073
BHQC	−6.09785	−1.81800	6.09785	1.81800	4.27984	3.95793	−3.95793	2.13992	0.46731	3.66023	0.27321
DFT/6-311++G**											
EHQP	−6.24370	−1.89010	6.24370	1.89011	4.35358	4.06691	−4.06691	2.17679	0.45939	3.79911	0.26322
BHQC	−6.16261	−1.87840	6.16261	1.87841	4.28419	4.02051	−4.02051	2.14210	0.46683	3.77306	0.26504

Table 11
Calculated quantum chemical parameters for protonated 5-substituted-8-hydroxyquinline molecules in gas phase (eV).

	E_{HOMO}	E_{LUMO}	I	A	ΔE	χ	μ	η	σ	ω	ε
HF/SDD											
EHQP	−12.43050	−2.92280	12.43050	2.92279	9.50773	7.67666	−7.67666	4.75387	0.21036	6.19824	0.16134
BHQC	−12.51820	−2.98760	12.51820	2.98756	9.53059	7.75286	−7.75286	4.76530	0.20985	6.30672	0.15856
HF/6-31++G**											
EHQP	−12.58700	−2.32410	12.58700	2.32414	10.2629	7.45557	−7.45557	5.13143	0.19488	5.41619	0.18463
BHQC	−12.72010	−2.45990	12.72010	2.45993	10.2601	7.59000	−7.59000	5.13007	0.19493	5.61474	0.17810
HF/6-311++G**											
EHQP	−12.61390	−2.31520	12.61390	2.31516	10.2988	7.46455	−7.46455	5.14939	0.19420	5.41030	0.18483
BHQC	−12.75380	−2.45390	12.75380	2.45394	10.2999	7.60387	−7.60387	5.14993	0.19418	5.61356	0.17814
DFT/SDD											
EHQP	−9.30555	−6.43200	9.30555	6.43200	2.87354	7.86878	−7.86878	1.43677	0.69600	21.5475	0.04641
BHQC	−9.96543	−6.47740	9.96543	6.47744	3.48798	8.22144	−8.22144	1.74399	0.57340	19.3786	0.05160
DFT/6-31++G**											
EHQP	−9.60025	−6.47580	9.60025	6.47581	3.12444	8.03803	−8.03803	1.56222	0.64012	20.67890	0.04836
BHQC	−10.05010	−6.50330	10.0501	6.50330	3.54676	8.27668	−8.27668	1.77338	0.56389	19.31440	0.05177
DFT/6-311++G**											
EHQP	−9.75373	−6.38740	9.75373	6.38737	3.36635	8.07055	−8.07055	1.68317	0.59412	19.34850	0.05168
BHQC	−10.09170	−6.55960	10.0917	6.55962	3.53207	8.32566	−8.32566	1.76603	0.56624	19.62500	0.05096

molecules in gas phase but generally there is no remarkable difference between them.

The initial molecule-metal interaction energy ($\Delta\psi$) is an important parameter, which has been determined by Sastri and al. [70] using the following Eq. (24):

$$\Delta\Psi = -\frac{(\chi_{Fe} - \chi_{inh})^2}{4(\eta_{Fe} + \eta_{inh})} \qquad (24)$$

Inspection of $|\Delta\psi||\Delta\psi|$ values listed in Tables 13 and 14 indicates that BHQC has the largest initial molecule-metal interaction energy than EHQP which correlates well with the experimental inhibition efficiencies.

The dipole moment is also another significant quantum chemical parameter when evaluating the adsorption ability of the organic inhibitor. Though, the literature reviews revealed that there is not a single decision on the relation between dipole moment and inhibition efficiency, some authors noted that the inhibition efficiency increases with increasing value of the dipole moment. Whereas other authors also reported that irregularities can be observed in the correlation between

dipole moment with inhibition efficiency. In our case, the classification of Inhibition efficiency according to the dipole moment values is not accordant with the experimental data. As can be seen from Table 15, there was no obvious correspondence between the values of the dipole moment for non-protonated and protonated molecules with the trend of protection efficiency obtained experimentally.

The studied 5-substituted-8-hydroxyquinline possessing heteroatoms such as oxygen and nitrogen can be easily protonated in the presence of an acidic solution. In order to measure of the basicity or of electron donating abilities of a chemical species, Proton affinity has been employed for both investigated molecules in gas phase and aqueous solution. So, the analysis of protonated forms of the investigated molecules is necessary to predict proton affinities of their non-protonated forms. It is worthy of note that an organic molecule with a high proton affinity acts as a good corrosion inhibitor. The proton affinity values of 5-substituted-8-hydroxyquinline in gas phase and aqueous solution using different calculation levels are listed in the Table 16, despite the fact that a few incompatibility exist mainly in the gas phase, the ranking of proton affinity values can be given as in the agreement with experimental findings presented: BHQC ˃ EHQP.

Table 12
Calculated quantum chemical parameters for protonated 5-substituted-8-hydroxyquinline molecules in aqueous solution (eV).

	E_{HOMO}	E_{LUMO}	I	A	ΔE	χ	μ	η	σ	ω	ε
HF/SDD											
EHQP	−9.48161	1.11377	9.48161	−1.11377	10.5954	4.18392	−4.18392	5.29769	0.18876	1.65215	0.60527
BHQC	−9.40242	1.12221	9.40242	−1.12221	10.5246	4.14011	−4.14011	5.26232	0.19003	1.62861	0.61402
HF/6-31++G**											
EHQP	−9.46719	0.99676	9.46719	−0.99676	10.4639	4.23521	−4.23521	5.23197	0.19113	1.71417	0.58337
BHQC	−9.3812	1.00329	9.38120	−1.00329	10.3845	4.18895	−4.18895	5.19225	0.19259	1.68976	0.59180
HF/6-311++G**											
EHQP	−9.55671	0.97989	9.55671	−0.97989	10.5366	4.28841	−4.28841	5.26830	0.18981	1.74539	0.57294
BHQC	−9.41739	0.97880	9.41739	−0.97880	10.3962	4.21929	−4.21929	5.19810	0.19238	1.71240	0.58398
DFT/SDD											
EHQP	−6.96236	−3.18080	6.96236	3.18076	3.78160	5.07156	−5.07156	1.89080	0.52888	6.80156	0.14703
BHQC	−6.95828	−3.17500	6.95828	3.17504	3.78323	5.06666	−5.06666	1.89161	0.52865	6.78550	0.14737
DFT/6-31++G**											
EHQP	−6.94304	−3.16200	6.94304	3.16198	3.78105	5.05251	−5.05251	1.89053	0.52895	6.75153	0.14811
BHQC	−6.87664	−3.17560	6.87664	3.17559	3.70105	5.02612	−5.02612	1.85052	0.54039	6.82560	0.14651
DFT/6-311++G**											
EHQP	−7.00127	−3.21610	7.00127	3.21613	3.78513	5.10871	−5.10871	1.89257	0.52838	6.89510	0.14503
BHQC	−6.93733	−3.23250	6.93733	3.23246	3.70486	5.08490	−5.08490	1.85243	0.53983	6.97899	0.14329

Table 13
Calculated quantum chemical parameters (ΔN_{maz}, $\Delta \psi$ and ΔE_{b-d} (in eV) and the optimized energies (E in hartree) of the non-protonated molecules under probe in gas phase and in aqueous solution (eV).

	Gas phase (non-protonated)				Aqueous (non-protonated)			
	ΔN_{max}	$\Delta \psi$	ΔE_{b-d}	E	ΔN_{max}	$\Delta \psi$	ΔE_{b-d}	E
HF/SDD								
EHQP	0.36287	−0.67892	−1.28901	−985.39494980	0.35242	−0.63623	−1.28068	−985.43974722
BHQC	0.37643	−0.72964	−1.28731	−911.76507126	0.35641	−0.64982	−1.27888	−911.79079520
HF/6-31++G**								
EHQP	0.35951	−0.59416	−1.14925	−985.74545164	0.35784	−0.60658	−1.18428	−985.77899401
BHQC	0.37522	−0.64090	−1.13802	−912.08897462	0.35954	−0.60866	−1.17711	−912.10826628
HF/6-311++G**								
EHQP	0.35636	−0.58358	−1.14887	−985.94048941	0.35372	−0.59206	−1.18302	−985.97325069
BHQC	0.37107	−0.62620	−1.13697	−912.26221816	0.35531	−0.59385	−1.17602	−912.28124445
DFT/SDD								
EHQP	0.69789	−1.08307	−0.55593	−991.46692570	0.68156	−1.01693	−0.54729	−991.50325854
BHQC	0.71913	−1.15155	−0.55668	−917.50609626	0.68292	−1.02068	−0.54712	−917.52807756
DFT/6-31++G**								
EHQP	0.69686	−1.07109	−0.55141	−991.68713190	0.68806	−1.02938	−0.54359	−991.71570047
BHQC	0.71587	−1.13027	−0.55138	−917.71138586	0.71079	−1.08114	−0.53498	−917.72752579
DFT/6-311++G**								
EHQP	0.71538	−1.12224	−0.54821	−991.90548872	0.67372	−0.98804	−0.54420	−991.93111588
BHQC	0.71370	−1.19261	−0.55161	−917.90515538	0.69546	−1.03606	−0.53552	−917.92126062

3.9. Monte Carlos simulations

Metropolis Monte Carlo simulation process allows determining the adsorption configurations and identified the lowest energy for the adsorption site of the adsorbate components (5-substituted-8-hydroxyquinline) on clean iron surface. The top and side views of the most stable adsorption configurations of BHQC and EHQP on Fe (110) surface using Monte Carlo simulations are shown in Fig. 15. It's appears from Fig. 15 that BHQC molecule adsorbed so that the heteroatoms of each moiety of the molecule could interact with the iron surface. However, the substituent at position 5 of EHQP molecule adsorbed to a parallel orientation on the iron surface, while the quinoline-ring system adsorbed a perpendicular orientation on the iron surface, this increase surface coverage and ensures strong interaction and therefore a high inhibition effect observed experimentally. The outputs and descriptors estimated by the Monte Carlo simulation, such as the total adsorption, rigid adsorption, and deformation energies, are listed in Table 17. The absorption energy is one of the most important parameters for adsorption; it is attributed to the energy released when the adsorbed adsorbate components are relaxed on the metal surface. The adsorption energy is defined as the sum of rigid adsorption and deformation energies of the adsorbate component. More negative adsorption energy value attribute to a big stabilized and strong interaction between adsorbed molecules and metal [71]. Another parameter dE_{ad}/dN_i has been reported in Table 17, which is corresponding to the energy of substrate-adsorbate configurations where one of the adsorbate components has been removed. As can be seen from the data in table that the negative values of adsorption energies of 5-substuted-8-hydroxyquinoline on the Fe (110) surface classified in the following order: BHQC > EHQP which is in good agreement with the experimental inhibition efficiency values.

Table 14
Calculated quantum chemical parameters (ΔN_{maz}, $\Delta \psi$ and ΔE_{b-d} (in eV) and the optimized energies (E in hartree) of the Protonated molecules under probe in gas phase and in aqueous solution (eV).

	Gas phase (protonated)				Aqueous (protonated)			
	ΔN_{max}	$\Delta \psi$	ΔE_{b-d}	E	ΔN_{max}	$\Delta \psi$	ΔE_{b-d}	E
HF/SDD								
EHQP	−0.07117	−0.02408	−1.18847	−985.80875365	0.26578	−0.37423	−1.32442	−985.84009212
BHQC	−0.07899	−0.02974	−1.19132	−912.17491808	0.27173	−0.38856	−1.31558	−912.19179722
HF/6-31++G**								
EHQP	−0.04439	−0.01011	−1.28286	−986.07730694	0.26422	−0.36526	−1.30799	−986.17160691
BHQC	−0.05750	−0.01696	−1.28252	−912.41864038	0.27070	−0.38047	−1.29806	−912.50127518
HF/6-311++G**								
EHQP	−0.04511	−0.01048	−1.28735	−986.27246123	0.25735	−0.34891	−1.31708	−986.36564401
BHQC	−0.04511	−0.01048	−1.28735	−912.59215010	0.26747	−0.37188	−1.29952	−912.67440556
DFT/SDD								
EHQP	−0.30234	−0.13133	−0.35919	−991.87912296	0.50995	−0.49171	−0.47270	−991.96158817
BHQC	−0.35019	−0.21387	−0.43600	−917.91296911	0.51103	−0.49399	−0.47290	−917.98647365
DFT/6-31++G**								
EHQP	−0.33223	−0.17243	−0.39055	−992.08459266	0.51506	−0.50154	−0.47263	−992.16512069
BHQC	−0.35996	−0.22977	−0.44334	−918.10505874	0.53333	−0.52637	−0.46263	−918.17689913
DFT/6-311++G**								
EHQP	−0.31802	−0.17023	−0.42079	−992.29787865	0.49966	−0.47251	−0.47314	−992.37973674
BHQC	−0.37532	−0.24877	−0.44151	−918.29814001	0.51692	−0.49497	−0.46311	−918.36983295

Table 15
Calculated Dipole Moment values for non-protonated and protonated 5-substituted-8-hydroxyquinline molecules in gas phase and aqueous solution using different calculation levels.

Basis set	HF/SDD		HF/6-31++G**		HF/6-311++G**		DFT/SDD		DFT/6-31++G**		DFT/6-311++G**	
	Gas phase	Aqueous phase	Gas phase	Aqueous phase	Gas phase	Aqueous phase	Gas phase	Aqueous phase	Gas phase	Aqueous phase	Gas phase	Aqueous phase
Dipole moment (non-protonated)												
EHQP	6.7748	10.8798	4.5353	9.2268	4.2642	9.0681	5.7413	11.8634	4.6177	10.2780	3.4924	10.1928
BHQC	4.2334	5.5659	3.3663	4.0538	3.3270	4.0021	4.0169	5.7124	3.3849	5.6802	3.3303	5.6404
Dipole moment (protonated)												
EHQP	9.6627	17.7048	9.3957	17.4850	9.3602	21.0096	9.5857	10.7509	9.8026	11.0033	6.9060	10.6919
BHQC	10.2000	16.8296	13.8879	17.2964	13.8252	17.2160	10.4860	13.5275	10.5795	16.4246	10.5119	16.3307

4. Conclusion

Two new compounds based on 5-aminomethyl-8-hydroxyquinoline were synthesized and characterized by IR, ^{1}H, ^{13}C NMR and Elemental analysis. The behavior of both compounds on the corrosion inhibition for carbon steel in 1 M HCl was investigated, from the obtained results and discussions; the following conclusions can be drawn:

- The results obtained from electrochemical methods demonstrated that the chemical structure of 5-alkylamino methyl-8-hydroxyquinoline has an influence on the inhibiting efficiency, and showed that BHQC and EHQP behave as mixed type corrosion inhibitors.
- The inhibition efficiency is connected to the concentration of 5-aminomethyl-8-hydroxyquinoline derivatives, and follows the sequence BHQC ˃ EHQP, but decreases with rise in temperature.
- One semicircle, corresponding to only one time constant, is observed in the impedance spectra with the introduction of BHQC and EHQP in both concentration and temperature experiments, the results obtained from electrochemical impedance spectroscopy measurement are compatible with those from potentiodynamic polarization.
- The adsorption of the BHQC and EHQP molecules on the carbon steel surface in 1 M HCl follows the Langmuir adsorption isotherm by forming a protective film which is confirmed by SEM investigation.
- The electronic absorption spectra of UV–visible confirm the formation of a complex that may also be responsible for the observed inhibition.
- Monte Carlo simulations show that the both molecules cannot adsorb in a similar manner on the iron surface following the order: BHQC > EHQP, which is in agreement with experimental ranking.
- The results obtained from Hartree Fock (HF), density functional theory (DFT) with different basis sets are somewhat in agreement with the experimentally determined inhibition efficiencies. These

data are important for the synthesis and rational design of new 5-substuted-8-hydroxyquinolines in the future studies.

Appendix A. Supplementary data

Supplementary data to this article can be found online at https://doi.org/10.1016/j.molliq.2019.01.105.

References

[1] A. Jafry, The CPO Goes to War Against Corrosion, The Economist, Morocco, N° 2159, 2005.
[2] D.B. Hmamou, R. Salghi, A. Zarrouk, H. Zarrok, R. Touzani, B. Hammouti, A. El Assyry, J. Environ. Chem. Eng. 3 (2015) 2031–2041.
[3] F. Bentiss, C. Jama, B. Mernari, H. El Attari, L. El Kadi, M. Lebrini, M. Lagrenée, Corros. Sci. 51 (2009) 1628–1635.
[4] S.V. Ramesh, A.V. Adhikari, Mater. Chem. Phys. 115 (2009) 618–627.
[5] H. Zarrok, A. Zarrouk, B. Hammouti, R. Salghi, C. Jama, F. Bentiss, Corros. Sci. 64 (2012) 243–252.
[6] R. Touir, R.A. Belakhmima, M.E. Touhami, L. Lakhrissi, M. El Fayed, B. Lakhrissi, M. Essassi, J. Mater, Environ. Sci. 4 (2013) 921–930.
[7] H. Zarrok, A. Zarrouk, R. Salghi, Y. Ramli, B. Hammouti, S.S. Al-Deyab, H. Oudda, Int. J. Electrochem. Sci. 7 (2012) 8958–80973.
[8] M. El Faydy, H. Lgaz, R. Salghi, M. Larouj, S. Jodeh, M. Rbaa, B. Lakhrissi, J. Mater, Environ. Sci. 7 (9) (2016) 3193–3210.
[9] H. Lgaz, R. Salghi, M. Larouj, M. El faydy, S. Jodeh, Z. Rouifi, H. Oudda, J. Mater. Environ. Sci. 7 (2016) 4471–4488.
[10] A. Zarrouk, H. Zarrok, R. Salghi, N. Bouroumane, B. Hammouti, S.S. Al-Deyab, R. Touzani, Int. J. Electrochem. Sci. 7 (2012) 10215–10232.
[11] F. Bentiss, M. Traisnel, H. Vezin, M. Lagrenee, Ind. Eng. Chem. Res. 39 (2000) 3732–3736.

Table 16
Calculated proton affinity values of studied quinoline derivatives in gas phase and aqueous solution using different calculation levels.

	Gas phase						Aqueous solution					
	HF/SDD	HF/6-31++G**	HF/6-311++G**	DFT/SDD	DFT/6-31++G**	DFT/6-311++G**	HF/SDD	HF/6-31++G**	HF/6-311++G**	DFT/SDD	DFT/6-31++G**	DFT/6-311++G**
EHQP	−3.90440	−1.67363	−1.67680	−3.86067	−3.45952	−3.32148	−3.53803	−3.32755	−3.32157	−5.11647	−4.87394	−4.85217
BHQC	−3.90669	−1.66403	−1.62127	−3.71573	−3.35641	−3.33767	−3.55592	−3.33833	−3.34247	−5.11828	−4.87266	−4.85085

Table 17
Outputs and descriptors calculated by the Monte Carlo simulation for the most stable adsorption configurations of 5-substituted-8-hydroxyquinline derivatives on Fe (110) surface (all units in kcal/mol).

Compounds	Total energy	Adsorption energy	Rigid adsorption energy	Deformation energy	3D Atomistic: dE_{ad}/dN_i
EHQP	−104.84328513	−121.60264496	−125.10470378	3.50205882	−121.60264496
BHQC	−108.13618165	−133.60057797	−117.46889109	−16.13168688	−133.60057797

[12] M. Elbakri, R. Touir, M.E. Touhami, A. Zarrouk, Y. Aouine, M. Sfaira, A. El Hallaoui, Res. Chem. Intermed. 39 (2013) 2417–2433.
[13] I.B. Obot, A. Madhankumar, Mater. Chem. Phys. 177 (2016) 266–275.
[14] A. Zarrouk, H. Zarrok, R. Salghi, B. Hammouti, F. Bentiss, R. Touir, M. Bouachrine, J. Mater. Environ. Sci. 4 (2013) 177–192.
[15] A. Zarrouk, B. Hammouti, R. Touzani, S.S. Al-Deyab, M. Zertoubi, A. Dafali, S. Elkadiri, Int. J. Electrochem. Sci. 6 (2011) 4939–4952.
[16] J.P. Bernal, E.R. de San Miguel, J.C. Aguilar, G. Salazar, J. De Gyves, Sep. Sci. Technol. 35 (2000) 1661–1679.
[17] Y.F. Cheng, D.T. Zhao, M. Zhang, Z.Q. Liu, Y.F. Zhou, T.M. Shu, C.H. Huang, Tetrahedron Lett. 47 (2006) 6413–6416.
[18] G. Achary, H.P. Sachin, Y.A. Naik, T.V. Venkatesha, Mater. Chem. Phys. 107 (2008) 44–50.
[19] Y. Abboud, B. Hammouti, A. Abourriche, A. Bennamara, H. Hannache, Res. Chem. Intermed. 38 (2012) 1591–1607.
[20] M. El Faydy, H. Lgaz, R. Salghi, M. Larouj, S. Jodeh, M. Rbaa, B. Lakhrissi, J. Mater, Environ. Sci. 7 (2016) 3193–3210.
[21] M. El Faydy, M. Galai, R. Touir, A. El Assyry, M.E. Touhami, B. Benali, B. Lakhrissi, A. Zarrouk, J. Mater, Environ. Sci. 7 (2016) 1406–1416.
[22] M. El Faydy, M. Galai, A. El Assyry, A. Tazouti, R. Touir, B. Lakhrissi, A. Zarrouk, J. Mol. Liq. 219 (2016) 396–404.
[23] H. Bougharrafa, R. Benallala, T. Sahdanea, D. Mondieigb, Ph. Negrierb, S. Massipc, M. El faydy, B. Lakhrissi, B. Kabouchia, Russ. J. Phys. Chem. A 2 (2017) 359–366.
[24] M. El Faydy, M. Galai, M. Ebn Touhami, I.B. Obot, B. Lakhrissi, A. Zarrouk, J. Mol. Liq. 247 (2017) 1014–1027.
[25] C. Adamo, D. Jacquemin, Chem. Soc. Rev. 42 (2013) 845–856.
[26] M.J. Frisch, G.W. Trucks, H.B. Schlegel, G.E. Scuseria, M.A. Robb, J.R. Cheese-man Jr., et al., Gaussian 03 W, Gaussian Inc, Wallingford, CT, 2004.
[27] R.D. Dennington, T.A. Keith, C.M. Millam, GaussView 5.0 Wallingford, CT, 2009.
[28] S. Kaya, C. Kaya, I.B. Obot, N. Islam, Spectrochim. Acta A Mol. Biomol. Spectrosc. 154 (2016) 103–107.
[29] W. Yang, R.G. Parr, Proc. Natl. Acad. Sci. 82 (1985) 6723–6726.
[30] R.G. Parr, P.K. Chattaraj, J. Am. Chem. Soc. 113 (1991) 1854–1855.
[31] T. Koopmans, Über die Zuordnung von Wellenfunktionen und Eigenwerten zu den Einzelnen Elektronen Eines Atoms, Physica, 1, 1933 104–113.
[32] W. Yang, C. Lee, S.K. Ghosh, J. Phys. Chem. 89 (1985) 5412–5414.
[33] R.G. Parr, L. Sventpaly, S. Liu, J. Am. Chem. Soc. 121 (1999) 1922–1924.
[34] L. Guo, S. Zhu, S. Zhang, Q. He, W. Li, Corros. Sci. 87 (2014) 366–375.
[35] H. Sun, J. Phys. Chem. B 102 (1998) 7338–7364.
[36] I. Ahamad, R. Prasad, M.A. Quraishi, Corros. Sci. 52 (2010) 1472–1481.
[37] S.A. El Rehim, M.A. Ibrahim, K.F. Khalid, Mater. Chem. Phys. 70 (2001) 268–273.
[38] A. Zarrouk, B. Hammouti, T. Lakhlifi, M. Traisnel, H. Vezin, F. Bentiss, Corros. Sci. 90 (2015) 572–584.
[39] M. Lebrini, M. Lagrenée, H. Vezin, M. Traisnel, F. Bentiss, Corros. Sci. 49 (2007) 2254–2269.
[40] R. Mehdaoui, A. Khelifa, A. Khadraoui, O. Aaboubi, A. Hadj Ziane, F. Bentiss, A. Zarrouk, Res. Chem. Intermed. 42 (2016) 5509–5526.
[41] R. Chami, F. Bensajjay, S. Alehyen, M. El Achouri, A. Bellaouchou, A. Guenbour, Colloids Surf. A Physicochem. Eng. Asp. 480 (2015) 468–476.
[42] H. Ouici, M. Tourabi, O. Benali, C. Selles, C. Jama, A. Zarrouk, F. Bentiss, J. Electroanal. Chem. 803 (2017) 125–134.
[43] M. Tourabi, A. Sahibed-Dine, A. Zarrouk, I.B. Obot, B. Hammouti, F. Bentiss, A. Nahlé, Prot. Met. Phys. Chem. Surf. 53 (3) (2017) 548–559.
[44] M. Chevalier, F. Robert, N. Amusant, M. Traisnel, C. Roos, M. Lebrini, Electrochim. Acta 131 (2014) 96–105.
[45] D.K. Yadav, D.S. Chauhan, I. Ahamad, M.A. Quraishi, RSC Adv. 3 (2013) 632–646.
[46] M. Kissi, M. Bouklah, B. Hammouti, M. Benkaddour, Appl. Surf. Sci. 252 (2006) 4190–4197.
[47] A. Zarrouk, B. Hammouti, A. Dafali, F. Bentiss, Ind. Eng. Chem. Res. 52 (2013) 2560–2568.
[48] F. Bentiss, M. Lebrini, M. Lagrenée, M. Traisnel, A. Elfarouk, H. Vezin, Electrochim. Acta 52 (2007) 6865–6872.
[49] A. Zarrouk, H. Zarrok, Y. Ramli, M. Bouachrine, B. Hammouti, A. Sahibed-dine, F. Bentiss, J. Mol. Liq. 222 (2016) 239–252.
[50] P. Mourya, P. Singh, A.K. Tewari, R.B. Rastogi, M.M. Singh, Corros. Sci. 95 (2015) 71–87.
[51] A. Popova, M. Christov, A. Vasilev, Corros. Sci. 49 (2007) 3290–3302.
[52] A. Popova, E. Sokolova, S. Raicheva, M. Christov, Corros. Sci. 45 (1) (2003) 33–58.
[53] H. Tayebi, H. Bourazmi, B. Himmi, A. El Assyry, Y. Ramli, A. Zarrouk, B. Hammouti, Der. Pharm. Chem. 6 (2014) 220–234.
[54] B. Zerga, B. Hammouti, M. Ebn Touhami, R. Touir, M. Taleb, M. Sfaira, I. Forssal, Int. J. Electrochem. Sci. 7 (2012) 471–483.
[55] M. El Faydy, R. Touir, M.E. Touhami, A. Zarrouk, C. Jama, B. Lakhrissi, F. Bentiss, Phys. Chem. Chem. Phys. 20 (30) (2018) 20167–20187.
[56] H. Zarrok, H. Oudda, A. El Midaoui, A. Zarrouk, B. Hammouti, M. Ebn Touhami, A. Attayibat, S. Radi, R. Touzani, Res. Chem. Intermed. 38 (2012) 2051–2063.
[57] F. Zhang, Y. Tang, Z. Cao, W. Jing, Z. Wu, Y. Chen, Corros. Sci. 61 (2012) 1–9.
[58] P. Mourya, S. Banerjee, R.B. Rastogi, M.M. Singh, Ind. Eng. Chem. Res. 52 (2013) 12733–12747.
[59] P.M. Wadhwani, D.G. Ladha, V.K. Panchal, N.K. Shah, RSC Adv. 5 (2015) 7098–7111.
[60] Y. Abboud, A. Abourriche, T. Saffaj, M. Berrada, M. Charrouf, A. Bennamara, H. Hannache, Desalination 237 (2009) 175–189.
[61] A. Popova, M. Christov, S. Raicheva, E. Sokolova, Corros. Sci. 46 (2004) 1333–1350.
[62] I.B. Obot, N.O. Obi-Egbedi, Corros. Sci. 52 (2010) 657–660.
[63] A. Zarrouk, I. El Ouali, M. Bouachrine, B. Hammouti, Y. Ramli, E.M. Essassi, I. Warad, A. Aouniti, R. Salghi, Res. Chem. Intermed. 39 (2013) 1125–1133.
[64] A. Domenicano, I. Hargittai, Accurate Molecular Structures, Their Determination and Importance, Oxford University Press, New York, 1992.
[65] I.B. Obot, S.A. Umoren, Z.M. Gasem, R. Suleiman, B. El Ali, J. Ind. Eng. Chem. 21 (2015) 1328–1339.
[66] R.G. Pearson, Acc. Chem. Res. 26 (1993) 250–255.
[67] R.G. Pearson, J. Am. Chem. Soc. 85 (1963) 3533–3539.
[68] N.A. Wazzan, J. Ind. Eng. Chem. 26 (2015) 291–308.
[69] B. Gomez, N.V. Likhanova, M.A. Dominguez-Aguilar, R.V.A. Martinez-Palou, J. Gasquez, J. Phys. Chem. 110 (2006) 8928–8934.
[70] V.S. Sastri, J.R. Perumareddi, Corrosion 53 (1997) 617–622.
[71] A.M. Kumar, R.S. Babu, I.B. Obot, Z.M. Gasem, RSC Adv. 5 (2015) 19264–19272.